TIME DOMAIN SEAKEEPING SIMULATIONS OF SOME MULTIPLE WATERPLANE VESSELS

D. BRADLEY RIXMANN

Your file Votre référence
ISBN: 0-612-84036-0
Our file Notre référence
ISBN: 0-612-84036-0

Time Domain Seakeeping Simulations of Some Multiple Waterplane Vessels

By

©D. Bradley Rixmann, B.A.Sc.

A thesis submitted to the School of Graduate Studies
in partial fulfillment of the
requirements for the degree of
Master of Engineering

Faculty of Engineering and Applied Science
Memorial University of Newfoundland

December, 2001

St. John's Newfoundland Canada

Abstract

In the design of ships and offshore structures, it is often desirable to assess the effects of environmental forces such as wind and waves on the vessel prior to its construction. Hence, several computational methods have been developed to predict the seakeeping performance of a prototype vessel in the design stage. Many of the commonly used methods are limited in their applicability to either vessel geometry or vessel operating conditions. The time-domain ship seakeeping simulation code, MOTSIM, has recently been extended for use with multi-waterplane vessels such as semi-submersibles and catamarans. As a further extension, the MOTSIM solver was modified to allow simulation of two vessels connected by a mechanical constraint such as an Articulated Tug Barge (ATB) Unit.

Some validation studies were carried out to validate the modifications to the MOTSIM code. Model test data for a triangular semi-submersible platform was compared against simulated results. Comparison between the experiment and simulations was generally good except for very low wave frequencies which was likely due to wave reflection in the model basin.

Similarly, simulations were performed for an ATB unit. Comparison of the connection loads and relative motion between the vessels appears quite reasonable for the limited set of simulations completed. Instability of the constraint algorithm caused a reduction in the number of simulations included in this study.

The results presented indicate a strong potential for the application of the MOTSIM seakeeping code to problems involving multiple waterplane vessels or multiple vessels in proximity. However, further validation work is needed to confirm the accuracy of the code for more general vessel geometries.

Acknowledgements

First, I would like to thank Dr. Don Bass for his mentoring in my studies, his patience and understanding as deadline after deadline drifted past, and his pointed warnings about spending my time appropriately.

I would also like to acknowledge the financial support of Marineering Limited for paying the many continuance fees as time passed by.

Thanks to Mike Doucet for his backhanded encouragement and prodding which help push me along to the end and for the healthy dose of red ink he applied to several drafts of this thesis.

To my parents, Don and Zelma Rixmann, for their encouragement, support and prayers both for me and my family while I spent too much time in front of my computer.

And most importantly, my deepest gratitude goes to my family. To my wife, Andrea, for her patience, strength, and encouragement when I needed it most, and to my children, Luke, Hunter and Hayley the many nights when Daddy didn't play with you or tuck you in. I will work less and be home more – I promise.

Table of Contents

List of Figures

List of Tables

Chapter 1

Introduction

In the design of ships and offshore structures, it is often desirable to assess the effects of environmental forces such as wind and waves on the vessel prior to its construction. Seakeeping performance is of significant importance in vessel design for a number of reasons. For all vessels, the motion and wave forces are important in designing the structure of the vessel. For passenger vessels, seakeeping is an important consideration for passenger comfort and seasickness avoidance. Similarly for cargo vessels, wave induced motions and accelerations affect the seafastening requirements for deck cargo such as containers or can cause cargoes to shift or slosh in bulkers or tankers. Slamming due to forefoot emergence can cause severe fatigue loading to a vessel's structure.

In the offshore oil and gas industry, seakeeping is particularly important due to the stationary nature of drill and production platforms such as the one shown in Figure 1. Knowledge of the anticipated wave forces is critical to the design of moorings and riser systems. Deck wetness due to waves can affect the safety and effectiveness of deck personnel. Platform motion can reduce the efficiency of process equipment and

jeopardize the safety of helicopter operations critical for crew safety. Given the issues identified here, many designers include some assessment of seakeeping in their design cycle using either physical experiments or computational simulations.

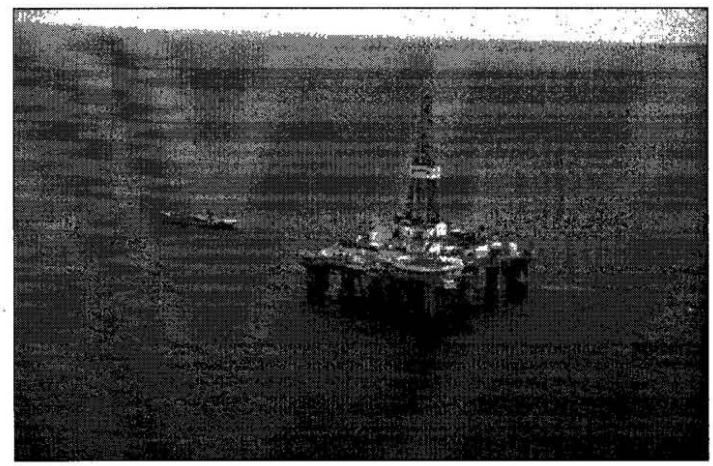

Figure 1: Photograph of a Semisubmersible Oil Platform

Traditionally, the evaluation of a prototype vessel's seakeeping performance was accomplished by physical experiments using scaled models in a towing or wave tank. This approach, however, requires that a detailed model be built including the complete hull geometry and that the mass properties of the model be scaled and set appropriately. This process can be very costly as models often cost tens of thousands of dollars to fabricate and outfit and model basin charges are currently on the order of several thousand dollars per day. In addition, the finite size of model test basins limits the size of waves which can be produced and often the duration of the test since wave reflection may occur and reduce the quality of the incoming wave train.

Within the past two decades, it has become practical to perform numerical simulations of vessels in waves. A variety of specific mathematical formulations are available, each of which has its own advantages and disadvantages. The general classes of numerical methods for seakeeping prediction are introduced in Chapter Two and a specific implementation, called MOTSIM, is described in Chapter Three. While these methods are well proven for conventional mono-hulled vessels, designs incorporating multiple waterplanes are becoming more commonplace. Chapters Four and Five of this thesis present a validation study of time-domain simulations using MOTSIM for some multiple waterplane vessels.

Chapter 2

State of the Art

2.1 Strip Theory

2.1.1 Overview

Currently, the most popular methods for computing the seakeeping performance of vessels are based on Strip Theory. Various forms of Strip Theory have been in use and development since the early 1950s (Beck, 1989). The essence of the method is the approximation of the three-dimensional fluid flow problem over a hull by a series of two-dimensional strips as illustrated in Figure 2 (Faltinsen, 1990).

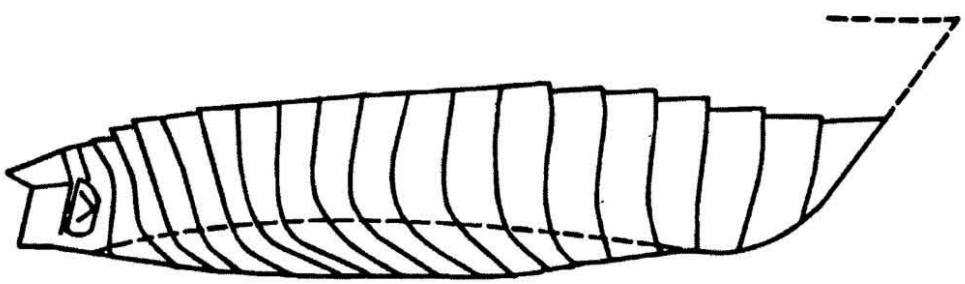

Figure 2: Illustration of Strip Theory for Ships (Faltinsen, 1990)

Many of the early methods were limited to zero speed, head seas or motion in the vertical plane only. During 1969 and 1970, several papers were published by different groups working independently which introduced more general forms of the theory including Söding (1969), Tasai and Takaki (1969) and Borodai and Netsvetayev (1969). The method described by Salvesen et al. (1970) has been the most widely accepted (Beck, 1989). This method includes prediction of heave, pitch, sway, roll and yaw motions as well as wave induced loads for a ship at constant speed at an arbitrary heading in regular waves. Vessel response in a general, random sea can be predicted from the regular wave results using the principle of superposition described by St. Denis and Pierson (1953).

Strip Theory is based on the assumption that the oscillatory motions of the vessel are linear and harmonic and occur at the frequency of the incident wave. In this method, all motions and force coefficients are computed as functions of frequency and so are generally said to be computed in the frequency domain (Oglivie, 1964). The principal differences between the various implementations of strip theory are typically in the corrections for forward speed.

There are three main stages to computing the ship's response using strip theory. First, the ship is divided into a number of transverse sections or strips, typically numbering twenty to forty. The two dimensional hydrodynamic coefficients (added mass, damping, wave excitation and restoring force) are computed for each section. These values are

then integrated along the length of the vessel to obtain the global coefficients for the coupled vessel motions. Finally, the equations of motion are solved algebraically.

Two methods are commonly used to calculate the hydrodynamic forces on the strips: Conformal mapping and Close-Fit methods. In the first method, the section coefficients are calculated by relating the actual section shape, via a conformal mapping, to that of a unit semi-circle for which the solution is known. Various methods have been proposed to perform this mapping such as those of Lewis (1929) and Ursell (1949). The most commonly used of these is based on the Lewis forms which use two parameters based on the sectional beam-to-draft ratio and the sectional area coefficient to define the mapping.

Close-fit methods are those which attempt to solve the potential flow problem directly on the actual sectional geometry using boundary integral techniques. The method of Frank (1967) is perhaps the most commonly used of these methods. The Frank Close-Fit method represents the section shape as a series of straight line segments. A series of fluid sources of constant but unknown strength are distributed along each segment. Applying the boundary conditions permits solution of the source strengths and hence the velocity potential on each segment. The pressure associated with the velocity potential is then integrated over the surface of the section to yield the added mass and damping coefficients.

While the formulation of strip theory assumes a long, slender vessel (Faltinsen, 1990), its use for alternate hull forms was anticipated by Salvesen et. al. (1970) over thirty years ago. The method has subsequently been applied to more complex hull forms

including catamarans and drilling platforms. The method has been proven to provide reliable estimates of motions and hull loads for a surprisingly wide range of hull forms and sea conditions as evidenced by the wide range of engineering software products in use today.

2.1.2 Advantages

The principal advantage of strip-theory is its speed and robustness. Using a computer code based on strip theory, it is possible to complete an exhaustive analysis of a vessel including response amplitude operators (RAOs) and irregular wave motion predictions for a range of headings in only a few minutes using a typical desktop computer at the time of this writing. Also, due to the relative simplicity of the input geometric data required – essentially sectional offsets, development of the model and preprocessing is very simple and efficient to complete.

The accuracy of strip theory is generally good for low Froude numbers and for higher frequencies. Its accuracy is particularly good in heave and pitch where the two-dimensional nature of the algorithm is most applicable.

The low computational cost of strip theory has contributed greatly to the popularity of this method among practical naval architects over the past decades as it was well adapted to the commonly available computer hardware during this time. As desktop computers become more and more powerful, it is reasonable to expect that users will migrate to the more complex computational approaches in search of more accurate results or more general applicability.

2.1.3 Limitations

The two-dimensional nature of strip theory makes it poorly suited to vessels which are not slender as the error in the two-dimensional approximation becomes more significant. Results are often poor for roll motions and for low encounter frequencies such as those experienced in following or quartering seas. Frequency domain computational method does not readily permit simulation of transient phenomena such as rudder actuation.

2.2 Three Dimensional Panel Methods

2.2.1 Overview

For large volume vessels or structures, the assumptions of strip theory are not applicable so another method of computing the wave structure interaction is required. Panel methods address this issue by solving the wave radiation potential over a set of three-dimensional panels.

To do this, the surface of the vessel is divided into triangular or quadrilateral panels. The potential flow is represented by a continuous distribution of pulsating sources over the wetted surface of the ship. The strength of the sources is assumed to be constant on each panel. To this point, the method is a logical extension of the strip theory methods discussed in the previous section. The methods required to solve the three-dimensional problem, however, are considerably more complex.

The velocity potential for the problem is given by:

$$\phi = \mathrm{Re}\left\{ \iint_{S_B} dsQGe^{-i\omega t} \right\} \tag{1}$$

where S_B is the surface area of the vessel, Q is the source density and G is the Green Function. The problem is solved by finding the Green Function which satisfies the boundary condition of impermeability on the vessel surface. Various methods of finding the Green Function have been developed by Wehausen and Latoine (1960), Abramowitz and Stegun (1964), and efficient computational methods have been developed by Newman (1985) and others.

A more advanced variation on the panel method is the Rankine Source Method. These methods avoid linearization of the free surface boundary conditions by distributing sources on all surfaces of a finite domain. For this reason, it is necessary to panel the wetted body surface, the free surface, as well as the bottom and sides of the domain. This formulation is often referred to as the numerical wave tank problem. These methods have proven very difficult to solve efficiently and require significant computational effort and thus are not very popular in a commercial sense.

2.2.2 Advantages

The most significant advantage of a panel method is the ability to handle complex, high volume geometric forms such as those associated with semi-submersible oil drilling platforms and large ships. These methods have been extensively verified and found to produce good results for a wide range of structures.

2.2.3 Limitations

Traditional panel methods are based on linear wave theory in the frequency domain. This limits their application to moderate wave conditions where the error in this simplification is small. Most leading, commercially available panel method packages are also limited to zero speed conditions. This limits their applicability to stationary structures or moored vessels. Newer methods are being developed which are applicable to non-linear and forward speed problems, but they are still very computationally expensive and have not been widely accepted as commercial tools to this point.

2.3 Navier-Stokes Methods

2.3.1 Overview

Computational Fluid Dynamics (CFD) is a blanket term which to some extent covers all the methods described herein. However, it has generally been accepted as referring specifically to those methods which involve the solution of some form of the Navier-Stokes equations. The Navier-Stokes equations are a complex set of equations for which only a handful of analytical solutions have been found. These equations include all macroscopic properties of a fluid including the effect of viscosity and as such are the focus of many research and development programs.

2.3.2 Advantages

The most distinct advantage of a CFD approach is that viscosity is not ignored. All the significant features of the flow around a body including those attributed to radiation, diffraction, mass forces and viscosity are accounted for. This approach should, then, provide a very accurate prediction of vessel forces and motions in a seaway.

2.3.3 Limitations

Unfortunately, the Navier-Stokes equations are quite expensive to solve. Accurate solutions often require more than one million control volumes. Even on the fastest computers available today, steady state solutions of such a magnitude require several hours of CPU time. Limited efforts, such as those of Stern et. al. at the Iowa Institute for Hydraulic Research, have been made to include the effect of waves in such simulations. In these cases, even solution of a few regular waves has required days of computational time.

With the rapid improvement of processor speed over the past several decades, it would be imprudent to discount CFD methods out of hand. It is clear, however, that these methods will not likely be practical for typical seakeeping problems for the next several years.

Chapter 3

MOTSIM

3.1 Overview

MOTSIM is a time-domain ship motion simulation code developed over the past decade or so by researchers at Memorial University of Newfoundland and the National Research Council of Canada's Institute for Marine Dynamics. The theoretical basis of this program has been described in detail by Pawlowski et. al. (1988) and again by Pawlowski and Bass (1991). This program solves the rigid body equations of motion for a floating body in the time domain. Hydrodynamic forces are computed over the instantaneous wetted surface of the vessel. The wave-ship interaction is computed by means of a non-linear formulation of the scattering potential. The Froude-Krylov force is computed at each time step based on the instantaneous wetted surface and body position. The implementation of this approach is described in the following paragraphs.

3.1.1 Geometric Representation

Unlike seakeeping methods based on linear theory which require only the geometry of the mean wetted surface of the vessel, MOTSIM requires that the entire hull geometry

to the uppermost watertight structure be entered. This is done so that the instantaneous wetted surface may be determined by the program during the solution. For moderate motions, it is typical to include the hull geometry up to the sheer line.

Hull geometry is represented in MOTSIM as strips, or sections, of quadrilateral or triangular panels. For each section, a local coordinate system is defined. The panels are defined by sets of offsets in the local YZ-plane and by the section width, ΔX. Since MOTSIM was originally developed for use with traditional monohull ships, the orientation of the local coordinate systems was assumed to be parallel with the ship fixed system. This restriction has been removed to allow modeling of more general geometric forms such as semi-submersibles. The modified format allows a local or component axis system to be defined with some arbitrary orientation to the ship system. This is accomplished by entering three unit vectors which define the direction of the local coordinate axes of the component system relative to the vessel frame and the coordinates of the origin of the section in the vessel frame as illustrated in Figure 3. Sections may be symmetric or asymmetric about their local XZ plane. Triangular panels are represented by repeating the coordinates of one of the corners in the offset data for the section.

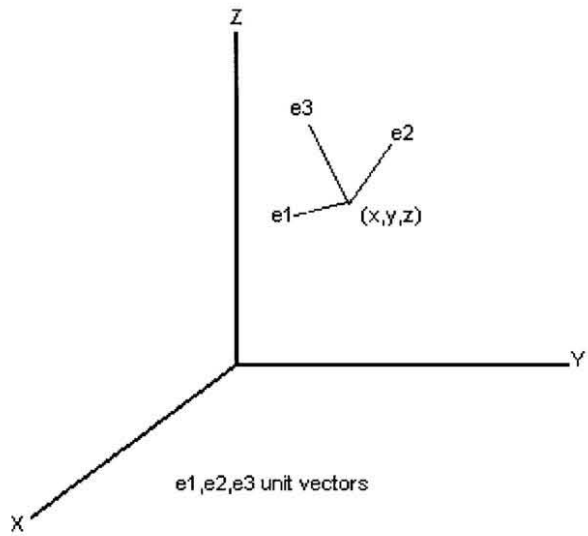

Figure 3: Definition of Local Coordinate System by Origin and Unit Vectors

To satisfy the requirements of the hydrodynamic calculations, panels are defined so that their normals are directed into the fluid domain. Based on the so-called right-hand-rule, this is accomplished by ensuring that the coordinates defining the corners of a panel are listed in counter-clockwise order when the panel is viewed from the fluid as illustrated in Figure 4. Since fluid pressures are integrated over the wetted surface of the body, it is necessary that the body volume be completely enclosed by panels.

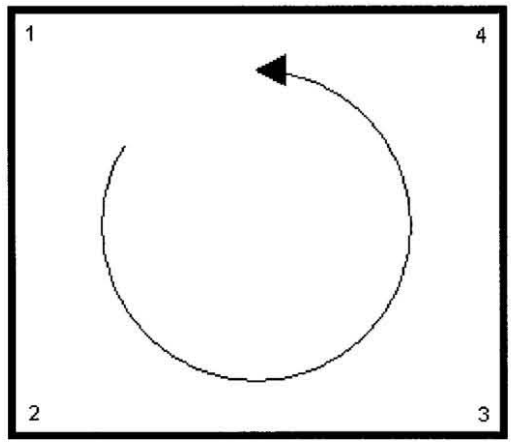

Figure 4: Counter-Clockwise Definition of Panel Nodes

3.1.2 Hydrodynamic Forces

3.1.2.1 Froude-Krylov Forces

The force induced on a body due to the undisturbed pressure field under a wave is known as the Froude-Krylov force. This force is the integral of the undisturbed wave pressure field over the wetted surface of the body. In MOTSIM, the Froude-Krylov force is computed at each time step using the instantaneous wetted surface of the vessel. The wetted surface is determined by finding those panels on the displaced body geometry which are fully or partially submerged. New panels are formed from the wet portion of the partially submerged panels so that they may be included in the computation. The Froude-Krylov force is then computed for each section by integrating the pressure using second order Gaussian quadrature.

3.1.2.2 Scattering Potential

The wave-body interaction forces are computed in MOTSIM in the time domain using a non-linear formulation of the scattering potential of the incoming wave. This

scattering potential is solved approximately using the method of modal potentials as described by Pawlowski and Bass (1991). The scattering potential represents a unified solution to the radiation-diffraction problem more commonly used to compute wave-body interactions. The implementation of this method in MOTSIM employs a linear free surface boundary condition with an approximate non-linear impermeability condition on the instantaneous wetted surface of the hull.

Added mass and damping coefficients are required by the MOTSIM time-domain solver for the evaluation of hull forces due to fluid flow as determined from the solution of the scattering potential. These values are obtained through preprocessing using a linear, frequency domain radiation solver of the type described in Chapter Two. To overcome the requirement of harmonic motion inherent in the frequency domain formulations, the added mass and damping coefficients are represented in the time domain implementation as memory or impulse-response functions. The use of these functions permits calculations with excitations of arbitrary frequency composition. The use of impulse-response functions is discussed with regard to time domain ship motion simulations by Ogilvie (1964).

3.1.2.3 Viscous Forces

In addition to the forces which can be computed using potential methods, viscous forces are significant in motions such as roll and yaw. A rigorous treatment of these forces would require solution of the Navier-Stokes equations which is very computationally expensive and is only recently becoming feasible for practical problems.

For this reason, much research has been done throughout the past century to quantify these forces and many empirical models have been developed to approximate their effect. Several such models have been implemented in MOTSIM to improve the accuracy of its predictions.

3.1.2.3.1 Roll Damping

Three methods of computing the viscous roll damping are included in MOTSIM. The first uses empirical coefficients determined from roll decay experiments. The remaining methods are semi-empirical models based on the work of Ikeda, as referenced by Himeno (1981), and on the work of Tanaka (1960). These empirical models are based on regression analysis of model test data. As it is generally accepted that eddy damping decreases with forward speed, corrections have been added to both models in MOTSIM to account for the effects of forward speed.

3.1.2.3.2 Drag

Vessels such as semi-submersibles often include portions of the hull which are relatively slender such as columns or pontoons. From Figure 5 it can be seen that viscous

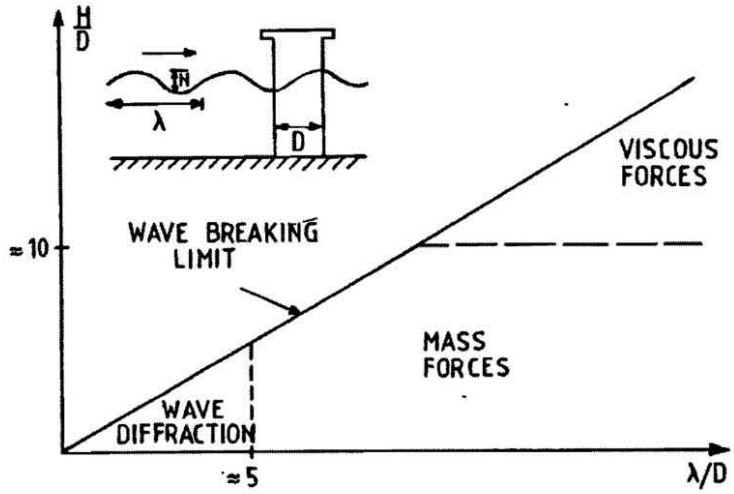

Figure 5: Relative importance of wave forces on marine structures (Faltinsen, 1990)

effects become significant when the wavelength is much larger than the characteristic dimension of the body geometry. For this reason, a drag formulation similar to that found in Morison's equation (Equation 2 for a circular cylinder) (Morison, 1950) is employed.

$$dF = \rho \frac{\pi D^2}{4} dL \cdot C_M \cdot a + \tfrac{1}{2} \rho C_D D \cdot dL |u| u \tag{2}$$

where dF is the force, u and a are the undisturbed fluid velocity and acceleration at the midpoint of the strip, D is the diameter, dL is the strip length and C_M and C_D are the mass and drag coefficients which must be determined empirically.

3.1.2.3.3 Maneuvering

Maneuvering forces are modeled in MOTSIM based on the work of Jacobs as reported in Mandel (1967). The forces and moments associated with drift, forward speed and yaw rate are computed based on formulae for calm water. The drift velocity and yaw rate are computed from equivalent modal velocity terms which reflect the motion of the vessel relative to the wave flow. The details of this implementation are discussed by Bass (1988).

3.1.2.4 Other Forces

The time-domain nature of the MOTSIM solver allows for easy implementation of additional models for forces acting on the vessel. Examples of these forces include the effects of propulsion systems, ride control systems or moorings.

3.1.3 Advantages

There are numerous advantages to the computational approach used by MOTSIM. The time-domain solution method allows simulation of non-harmonic motion including transient effects due to individual wave impacts or of control inputs. This effect is most significant in oblique seas where it is possible to account for the effects of yaw, leeway angle, rudder action, skegs, and other forces which influence the vessel motion. In addition, the non-linear implementation of the Froude-Krylov force evaluation permits simulation of motions in more extreme sea conditions than is appropriate using the purely linear methods. Finally, the time-domain output from MOTSIM is directly analogous to

the data obtained during wave tank tests which is generally more intuitive than the frequency domain output produced by most other approaches.

3.1.4 Limitations

One of the principal disadvantages of this method is the computational time required to produce a useful duration of output. Since the output is time-domain, a large number of time-steps must be completed to produce a statistically significant result. This disadvantage is particularly evident for simulations in irregular seas where several hundred wave encounters are required with run times of several hours. Since it is necessary to compute the added mass and damping coefficients during preprocessing, MOTSIM takes considerably longer than most frequency domain codes. It should be noted that this disadvantage is being offset by the rapid improvement of computer processor speed and it is now possible to complete a fairly comprehensive set of simulations overnight for a typical vessel.

Chapter 4

Time Domain Simulation of a Triangular Semi Submersible Platform

4.1 Introduction

As global oil exploration moves to the more extreme environments of deep water and into arctic regions, the cost of drilling and production increase substantially. The increase in production cost in these environments is making smaller fields in less extreme environments which were once thought to be uneconomic to produce more viable. To minimize the cost of developing small offshore oil and gas fields, smaller, more efficient drilling and production platforms are needed. To meet this demand, a number of novel concepts have been developed within the past decade or so. One example of this type of platform is the triangular semi-submersible.

This style of platform is triangular in shape and requires only three main columns instead of the four or more usually found on conventional semi-submersibles. This results in a cheaper vessel due to decreased steel weight and associated fabrication costs. As well, the waterplane area is decreased, likely decreasing motions which results in a lifetime cost savings due to an expanded weather window for drilling operations. Fewer

columns should also decrease lateral environmental forces due to waves and current thus requiring a lighter and less expensive mooring system with fewer legs. As in any engineering optimization, these benefits must be carefully balanced against their potentially detrimental effects.

Oceanic Consulting Corporation of St. John's, Newfoundland recently conducted model scale experiments to establish the hydrodynamic performance of one particular example of this type of semi-submersible platform (Harris, et. al. 1999). The concept design for the vessel consisted of an equilateral triangular ring pontoon with a single circular column at each corner joining it to a triangular deck. Three smaller diameter columns extended from the pontoon to the deck at the mid-span of each side of the vessel. Each vertex of the triangular shape was truncated slightly such that the resulting shape was hexagonal as seen in Figure 6. The test program had the following objectives: to characterize the vessel response in waves for the operating draft, to determine current loading on the vessel at the operating draft, and to determine its motion response and towing force in calm water and waves at transit draft. In the present work, the focus is on those aspects of the tests related to seakeeping. It should be noted that some vessel particulars are omitted in this document in the interest of client confidentiality.

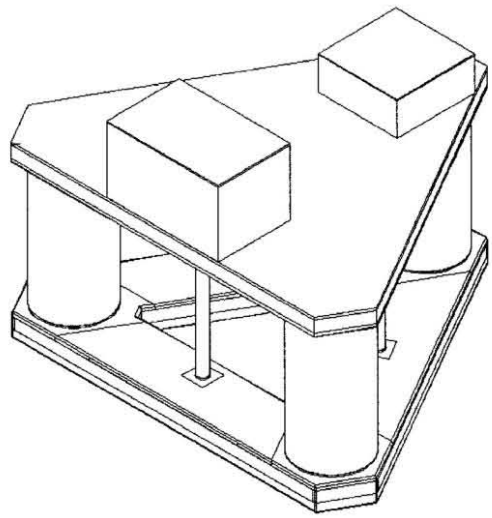

Figure 6: General Arrangement of Triangular Semi Model

A scale model was constructed and tested in regular and irregular seas at wave headings of 180, 150 and 120 degrees while restrained by a compliant spring mooring. The motions of the body, the mooring forces and other relevant parameters were recorded during the tests. In this chapter, the results of that study are compared to those computed by the MOTSIM seakeeping simulation software package to assess the suitability of the software for the characterization of novel semi-submersible designs.

4.2 Model Tests

4.2.1 Introduction

Oceanic Consulting Corporation designed and constructed a scale model of the concept semi-submersible platform. This model was used in seakeeping experiments conducted primarily in the Ocean Engineering Basin (OEB) at the National Research Council of Canada's (NRC) Institute for Marine Dynamics (IMD). The details of the experimental program are described below.

4.2.2 Model

The model was constructed at a scale of about 1:40. This value was selected for convenience in fabrication; in this case to facilitate the utilization of available sizes of stock material. The model consisted of three major components: the pontoon, the columns and the deck. The pontoon included an aluminum structure for strength and stiffness while the external shape of the pontoon was formed primarily from Styrofoam™. Renshape® (a polymer based composite modeling material) and aluminum were used in the regions where the columns mated with the pontoon. The pontoon was wrapped with three layers of woven fiberglass boat cloth secured with epoxy resin, then hand faired, sanded and painted. The cylindrical main columns were rolled from aluminum sheet with flanges welded into each end and a continuous weld along the longitudinal seam. The columns bolted to the aluminum mating surfaces at the top of the pontoon. Stock aluminum tubing was used for the smaller, intermediate columns. The bottom of these columns were inserted into pockets cut in the top face of the pontoon. The model's deck was made of plywood with only the bottom and sides enclosed. Acrylic boxes were installed on the upper deck to protect the instrumentation as indicated in Figure 6.

4.2.3 Test Facilities and Instrumentation

4.2.3.1 Ocean Engineering Basin

All moored seakeeping tests were performed in the Ocean Engineering Basin at the Institute for Marine Dynamics of the National Research Council of Canada located in St. John's, Newfoundland. This tank, illustrated in Figure 7 measures approximately

70m long by 30m wide by 3.5m deep. It features segmented, piston type, hydraulically actuated wave boards along its south and west sides and mesh type wave absorbers along the north and east sides. The wave making system is capable of generating regular wave heights up to one-metre and irregular spectra of up to 0.5 metre significant wave height. The progressive mesh beach systems minimize interference from reflected waves during tests. This tank also includes a current making system capable of providing a current speed of 0.25m/s at a water depth of 2.0m (the speed varies with water depth). To complete the environmental model, fans can be mounted above the water surface in the tank to generate wind in a localized region of the basin.

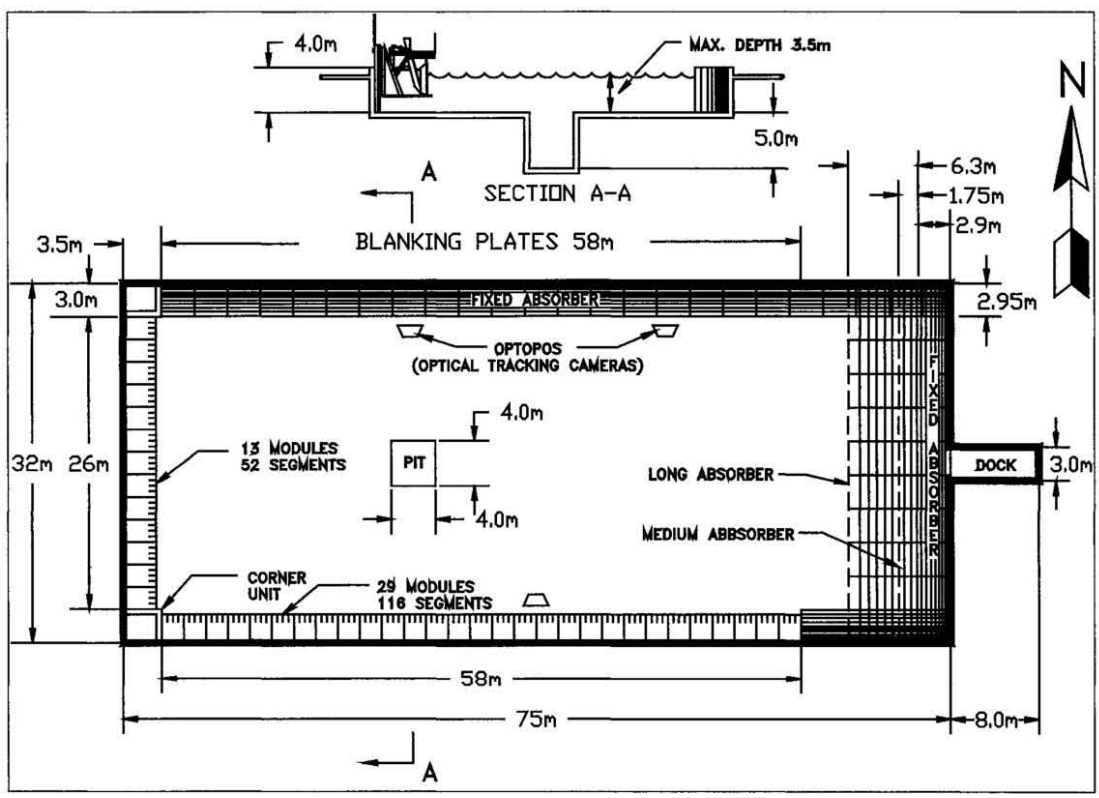

Figure 7: Schematic of IMD Offshore Engineering Basin

4.2.3.2 Motion Measurement

Model motion was recorded using Qualysis, an earth fixed optical tracking system. This system consists of two infrared cameras mounted on towers placed at known locations in the tank and a "tree" of six spherical reflectors attached to the model. The relative locations of the reflectors in the tree are known and are entered into the tracking software on a computer. During operation, the software acquires the images from the two cameras at a standard television frame rate of approximately 30Hz. The software computes the best fit between the known reflector positions and those appearing in the acquired image for each camera. Using this information and the known locations of the cameras, the system computes the location of the model relative to the tank. Linear displacements are referenced to the tank or earth fixed coordinate system, while angular displacements are referenced to a model fixed coordinate system that rotates (i.e. yaws) with the model.

In this case, the reflector tree was installed on the top of the deckhouse just aft of the longitudinal centre of gravity. This location was selected because it provided the best visibility of the reflector tree.

4.2.3.3 Accelerations

Accelerations on the model were measured using Motionpak, a compact assembly of three orthogonal accelerometers and angular rate gyros. This unit was installed on the main deck at a position forward of the longitudinal centre of gravity and was aligned on the model such that it recorded heave, surge and sway accelerations and roll, pitch and

yaw angular velocities. This device uses a right hand coordinate system that has the z-axis pointing downward and it rotates with the model.

4.2.3.4 Mooring System

In full-scale operation, the subject platform would be moored using a catenary mooring system. It was not practical to model this mooring in the basin, however, due to the water depth so a soft spring mooring system was used to maintain the model's long-term average position in the tank. The mooring was designed to be sufficiently compliant so as not to introduce significant loads and interfere with model motions at typical wave frequencies, hence the response of the model is representative of an unmoored model. In practice, the deepwater catenary mooring is expected to alter the response by adding damping and stiffness, especially in the vertical modes (i.e. heave, pitch and roll).

The soft spring mooring system consisted of a four-point tether arrangement for the 180° and 120° headings, and a three-point tether arrangement for the 150° heading. Thin stainless steel wires connected the mooring fairleads on the model to anchor points located on the tank walls or on towers in the tank. At each anchor point pulleys directed the line to a vertically mounted spring with a stiffness of 30 N/m. Each mooring line was pre-tensioned with approximately 15 N of force to provide an initial spring extension of 0.5 m (see Figure 8). Figures 9, 10 and 11 (from Harris et. al., 1999) show the mooring configurations for wave headings of 180, 150, and 120, respectively.

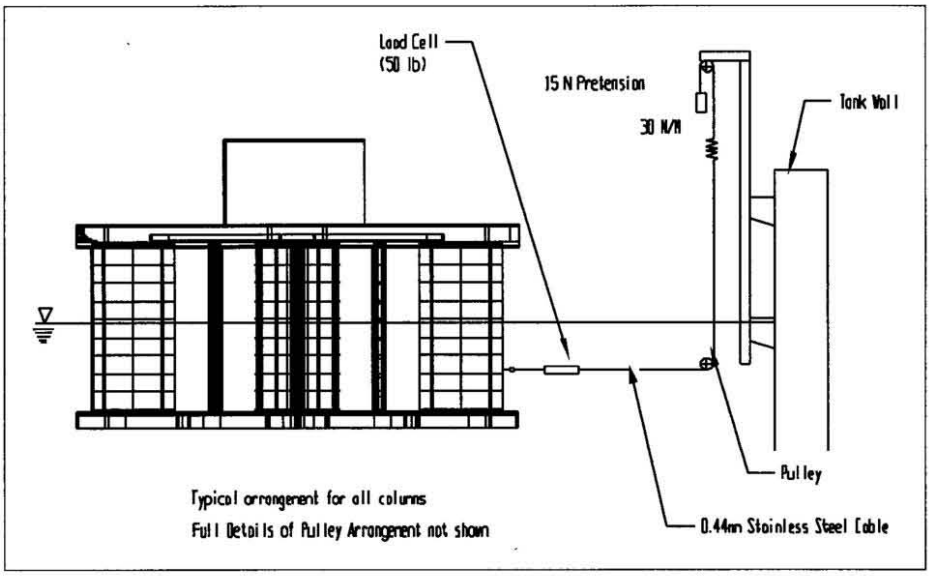

Figure 8: Model Test Mooring Leg Detail

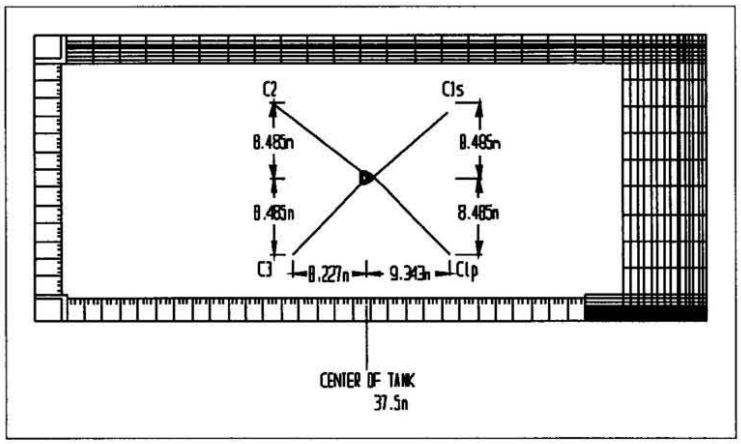

Figure 9: Mooring Arrangement for 180 Degree Wave Heading

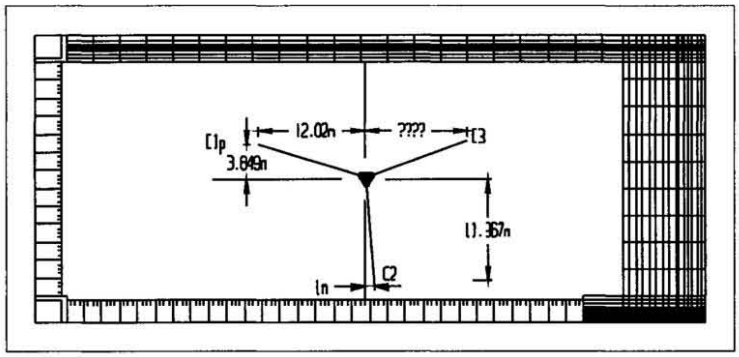

Figure 10: Mooring Arrangement for 150 Degree Wave Heading

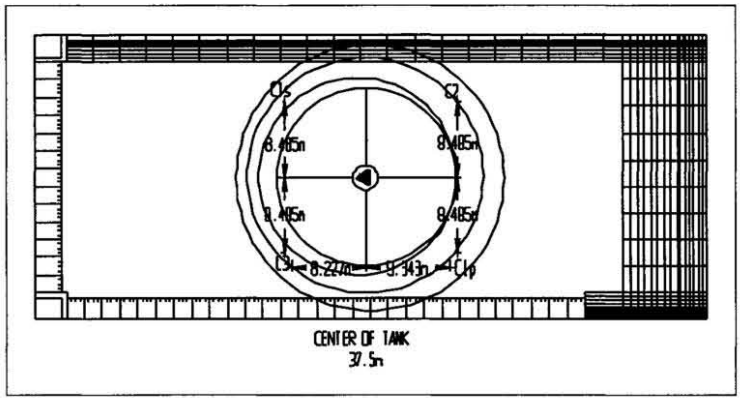

Figure 11: Mooring Arrangement for 120 Degree Wave Heading

To analyze the mooring loads, the positions of the fairleads (in tank coordinates) were computed from the measured model position and the line of action of each mooring line was calculated using the known anchor positions in the tank. The forces and moments from these loads were summed as vectors in the horizontal plane and resolved into the global (tank) coordinate system as the mooring restoration X load, Y load and yawing moment.

4.2.3.5 Wave Elevation

Wave ride-up was measured using five capacitance wave probes as indicated in Figure 12. One probe was located on each of the three main columns of the model. The fourth probe was placed on the port side of the model at the planned location of the risers and the fifth probe was placed under the deck at the geometric centre of the model.

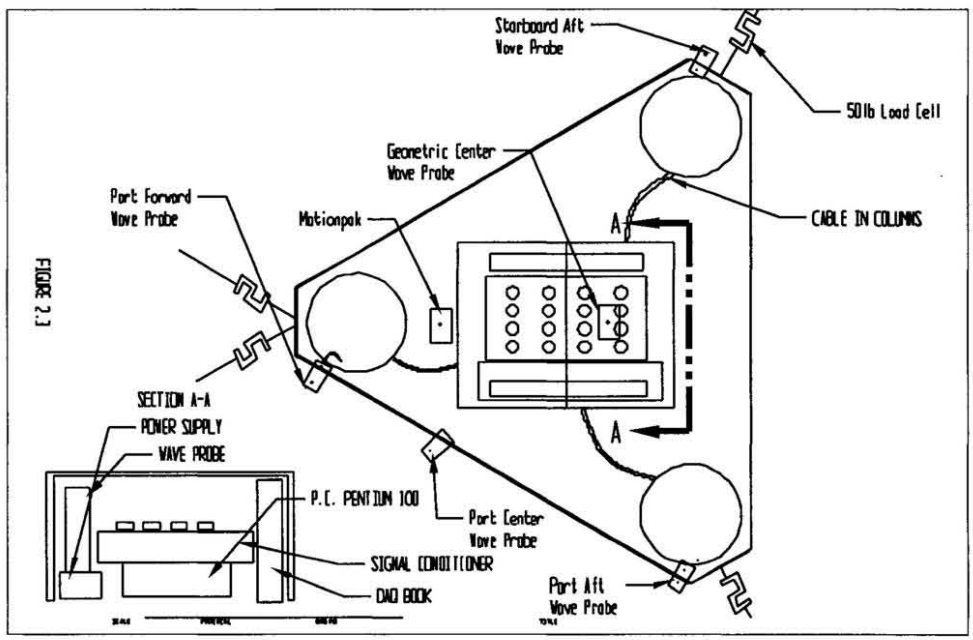

Figure 12: Instrumentation Arrangement for Tests in Waves (Harris et.al.,1999)

4.2.4 Seakeeping Experiments

4.2.4.1 Model Verification

For the tests described in this thesis, the model was configured to represent the planned operating draft of the full-scale prototype. Semi-submersible platforms are generally operated at a relatively deep draft to ensure that the pontoon remains well submerged in order to take advantage of the reduced motion response of the reduced

waterplane area of the columns. To ensure that the model mass properties were set correctly, the model was swung and inclined prior to the tests. Swinging involves placing the model in a frame of known mass distribution and dimensions. This frame has a pair of knife edges which serve as pivots. The model and frame are first inclined statically to allow computation of the location of the centre of gravity. The frame is then released thus imparting a swinging motion to the system. The period of the swinging motion is recorded either by multiple manual observations with a stopwatch or using the output of an inclinometer installed in the model. From this period, the mass moment of inertia of the system can be easily determined using Equation 3. Since these data are known for the swing frame, the contribution of the frame can be subtracted from the measured values to yield the required model properties.

$$I = \left(\frac{T}{2\pi}\right)^2 gM(z_{pivot} - z_{CG}) \tag{3}$$

As a final check, an inclining experiment was conducted with the outfitted model floating in the test basin. An inclining is performed by applying a known moment to the model about an axis in the horizontal plane and recording the resulting angle of inclination about that axis. The known moment is usually applied by moving a known mass a measured distance across the deck of the model. The vertical distance between the centre of gravity and the metacentre can then be calculated using the following relations:

$$GM_T = \frac{M_x}{\nabla \sin\varphi} \tag{4}$$

$$GM_L = \frac{M_y}{\nabla \sin\theta} \tag{5}$$

To verify the installation, heave, pitch, and roll decay experiments were performed for each mooring configuration and also with the model free of the mooring. Personnel located directly above the model applying an appropriate static force imposed an initial vessel displacement. The model was then released and the resulting motion was recorded.

4.2.4.2 Regular Waves

All regular waves were measured at the tank origin without the model in place to verify wave quality. The initial twelve waves were run and measured prior to model installation. The next five waves were used to better define the RAO curve. These were calibrated after the test program was completed. Seventeen regular wave experiments were conducted for the 180° heading; twelve of these defined the overall response while the remaining five waves were used to further define vessel response near the heave natural period. For the 150° and 120° headings, the shortest and longest waves were eliminated from the test program.

There was some concern that non-linear behavior may have been evident due to pontoon emergence in some of the longer and larger waves. At the 18 seconds period, a second wave was tested with a 1/60 wave slope. The normalized heave RAO response was identical to the previous 1/33 slope wave indicating that any non-linear response due to high wave height was insignificant.

4.2.4.3 Irregular Waves

Three long-crested irregular wave sets were calibrated with a return period of 1752 seconds, model scale, or 3 hours, full-scale. All irregular waves had a JONSWAP spectrum with peak enhancement value, γ, of 2.2. Three irregular waves were tested corresponding to a significant wave height (H_s) of 4.40 m, 6.95 m and 12.92 m, full scale. The irregular wave tests were conducted at wave headings of 180, 150 and 120 degrees at the operating draft.

4.3 Numerical Simulations

4.3.1 Model Preparation

4.3.1.1 Geometry

The form of the pontoon and main columns of the semi-submersible platform were converted to the MOTSIM geometric format. The deck was not represented as it was not expected to be wet during any part of the simulations. The initial mesh used for these simulations is shown in Figure 13. Since MOTSIM requires geometric data to be defined using sections with parallel sides, it was necessary to use several component or local coordinate systems to model the platform.

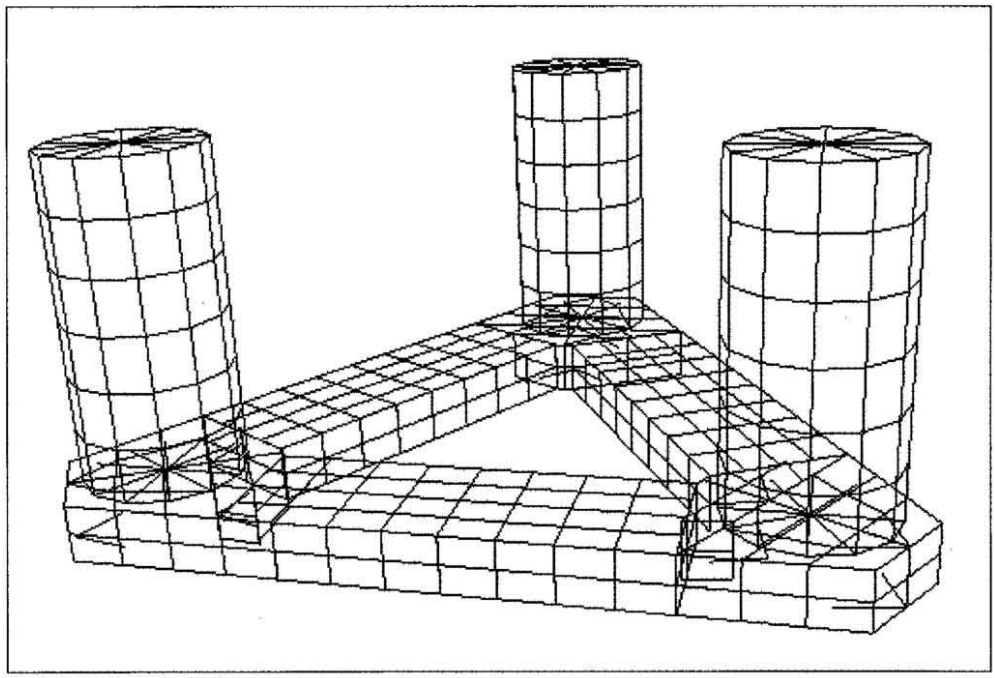

Figure 13: Initial MOTSIM Mesh for Triangular Semi-Submersible

The first coordinate system was rotated so that the X' axis pointed in the positive Z direction and Z' in the negative X direction. This coordinate system was used to define the circular walls of the main columns. Similarly, three coordinate systems were formed for the prismatic portions of the pontoon between each pair of main columns and three additional coordinate systems were used for the region of the pontoon beneath the main columns. Each coordinate system is defined by a set of three unit vectors which define the direction in the global frame of the x,y and z axes, respectively, as described in Chapter 3.

4.3.1.2 Preprocessing

Added mass and damping coefficients were computed for the model using MOTSIM's three dimensional radiation solver, 3DCOLD. These coefficients were evaluated at twenty-eight frequencies over the range 0.2 to 3.0.

4.3.2 Verification

4.3.2.1 Hydrostatics

To confirm the quality of the discretized model geometry, the MOTSIM solver was used to compute standard hydrostatic quantities for the vessel for comparison to those obtained by other calculations and through model test measurements.

Initially, the displaced fluid volume was computed for the operational draft in calm water with the vessel upright. Output from this computation also included net forces and moments acting on the vessel. Originally, a net yawing moment was indicated. Investigation of the sectional forces identified that the flat sections used to close the ends of the column/pontoon junctions were entered incorrectly. These sections were redefined and the computation repeated with the desired results.

The transverse and longitudinal metacentric heights were calculated from the restoring moments computed with one degree of roll and pitch respectively using Equations 4 and 5.

To ensure the quality of the panels, additional hydrostatic calculations were completed with the model fully submerged at different orientations. Because the net vertical force on the vessel (indicative of the displaced fluid volume) should be constant

at any orientation for the fully submerged case, this test provides a useful check for a correctly discretized geometry. It was found that the net vertical force with ninety degrees of pitch was about half that of the upright or rolled cases. Investigation of the geometric data indicated that the normals were incorrectly calculated for several of the flat sections closing the ends of the pontoons and joint regions under the main columns. Again, these sections were redefined and the verification process was repeated.

4.3.2.2 Free Decay Simulations

As for the model tests, decay simulations are useful to ensure the proper setup of the numerical model as well as being a good indicator of agreement between the two methods. These simulations are performed in a manner analogous to the physical tests; the vessel is given an initial perturbation from the equilibrium position and released in calm water and the motions are computed. Figures 14 through 16 show the initial results of the heave, pitch and roll decay simulations respectively for this vessel.

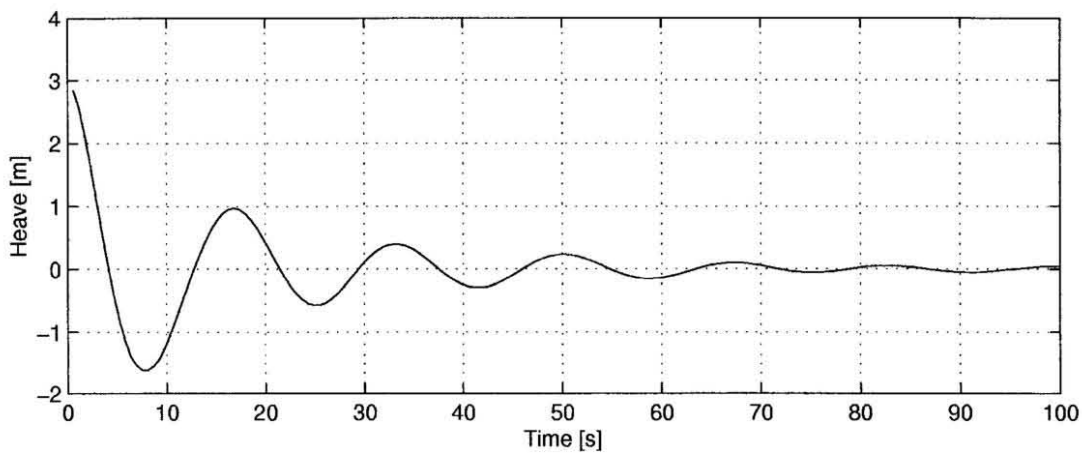

Figure 14: Heave Decay Simulation Results

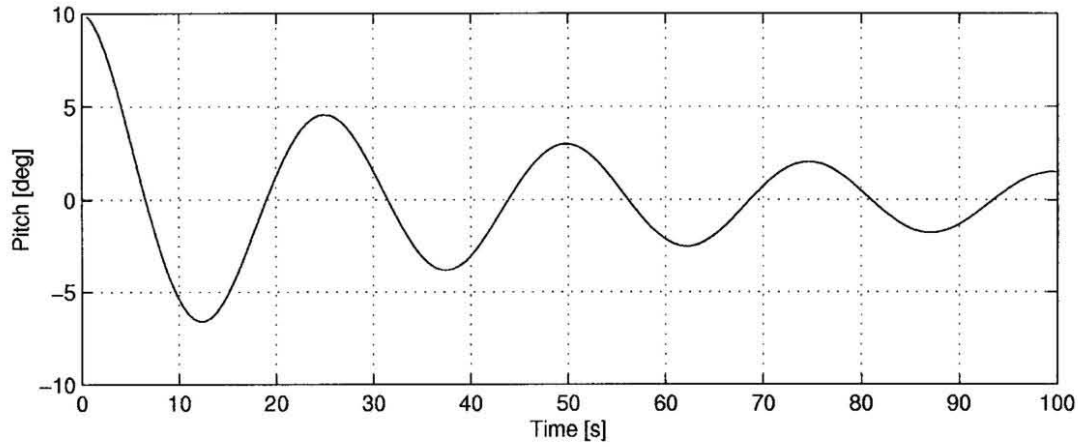

Figure 15: Pitch Decay Simulation Results

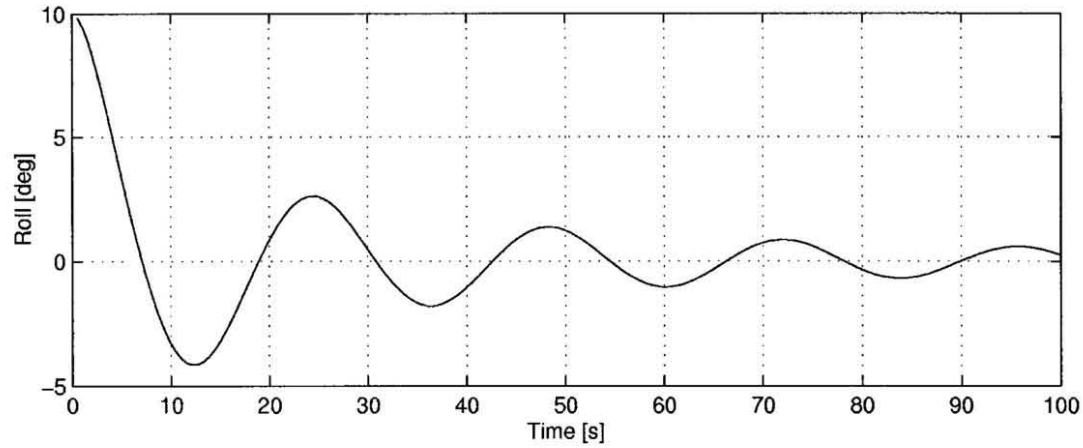

Figure 16: Roll Decay Simulation Results

Comparison with the natural periods reported in the previous section indicates significant variation between the experimental and computed values. In particular, the computed heave natural period was about two and a half seconds shorter than the measured value. Since the natural period oscillations of a vessel are basically analogous to that of a simple harmonic oscillator, Equation 6 below can be used to help deduce the likely sources of error in this calculation.

$$\frac{d^2\psi}{dt^2} + \omega_0^2 \psi = 0 \tag{6}$$

where:

$$\omega_0 = \sqrt{\frac{k}{m}} \tag{7}$$

substituting the heave restoring force and the virtual mass and converting frequency to period gives:

$$T_0 = 2\pi \sqrt{\frac{m_{vessel} + A_{33}}{\rho g A_{WP}}} \tag{8}$$

From this equation, the likely errors would be in the restoring force and the total mass. For heave motion, the restoring force is proportional to the waterplane area of the vessel as indicated by:

$$F_z = \rho g A_{WP} \Delta z \tag{9}$$

Where F_z is the heave restoring force and A_{WP} is the waterplane area at the nominal draft. For the prototype vessel, the waterplane area is simply the sum of the waterplane areas of the six circular columns, or:

$$A_{WP} = \frac{3}{4}\pi\left(D_{main}^2 + D_{Intermediate}^2\right) \tag{10}$$

Comparison of this value to that obtained from MOTSIM indicated that the waterplane area of the discretized geometry was about 5% lower than the required value. This error was found to be due to the way in which the columns were discretized. The

circular cross section was represented by a twelve sided equilateral polygon inscribed in a circle with the column diameter, similar to that shown in Figure 17. The error associated with the polygon approximation of a circle is represented by the shaded area.

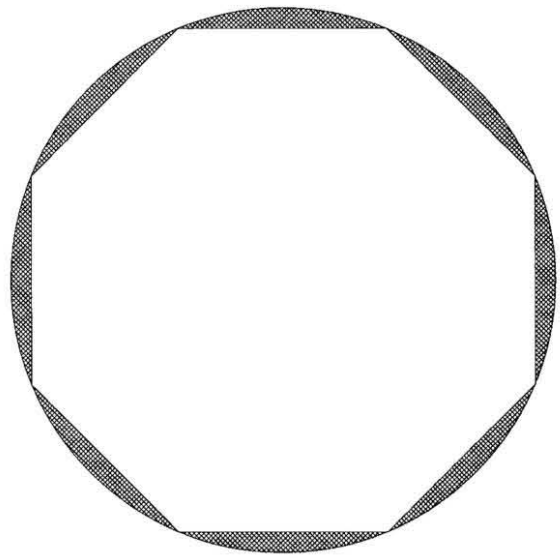

Figure 17: Illustration of Error in Discretization of Circular Section

For traditional ship geometries discretized using the inscribed polygon method, with a reasonable number of panels, the error is typically on the order of two percent of total displacement. For a circular section, the error associated with an n-sided inscribed polygon can be calculated from the relation:

$$\%Error = \left[1 - \frac{n}{\pi}\sin\left(\frac{\pi}{n}\right)\cos\left(\frac{\pi}{n}\right)\right] \times 100\% \tag{11}$$

Since a large number of panels would be needed to get a close match to the cross-sectional area, this approach was not well suited to this geometry. Instead, the polygon

diameter to give the same cross sectional area as a circular section was calculated using the relation:

$$R = \sqrt{\frac{\pi r^2}{n \cdot \sin\left(\frac{\pi}{n}\right)\cos\left(\frac{\pi}{n}\right)}} \tag{12}$$

The equivalent polygon diameter was used to correct the panelization of the main and intermediate columns. These corrections had the effect of increasing the stiffness of the heave restoring force. They were expected to further decrease the computed natural period and increase the discrepancy between the experimental and computed results. Figure 18 shows the revised calculations with the original added mass and damping values.

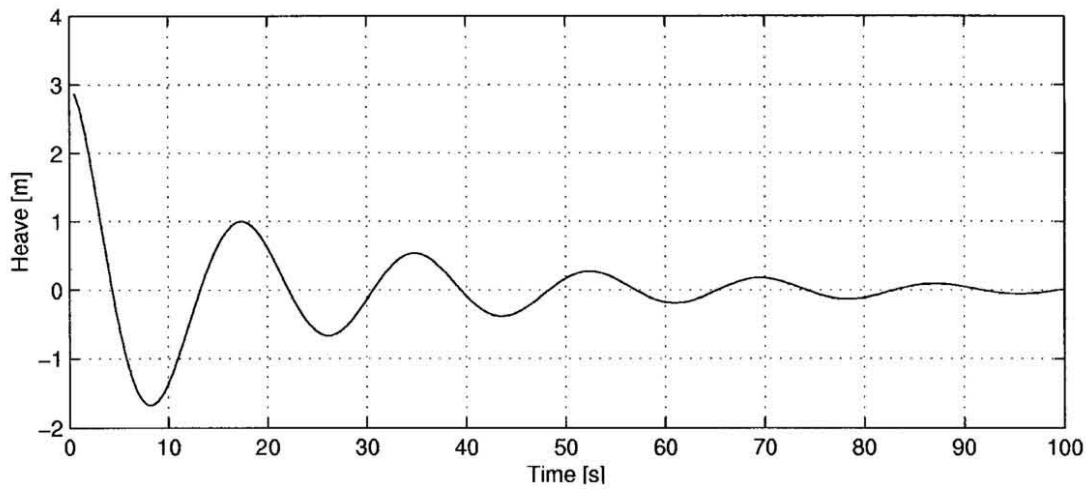

Figure 18: Heave Decay with Modified Column Geometry

We now turn our attention to the mass component of Equation 8. To increase the period, a significant increase in the total effective mass of the vessel is needed. Since the

required vessel mass is known, it is easy to verify that it is set correctly. The displaced mass of the vessel increased slightly due to the changes made to the discretization of the columns, however, as Figure 18 demonstrates, this does not have a significant effect on the heave period, rather a more substantial increase in the mass is required which must be due to the hydrodynamic added mass.

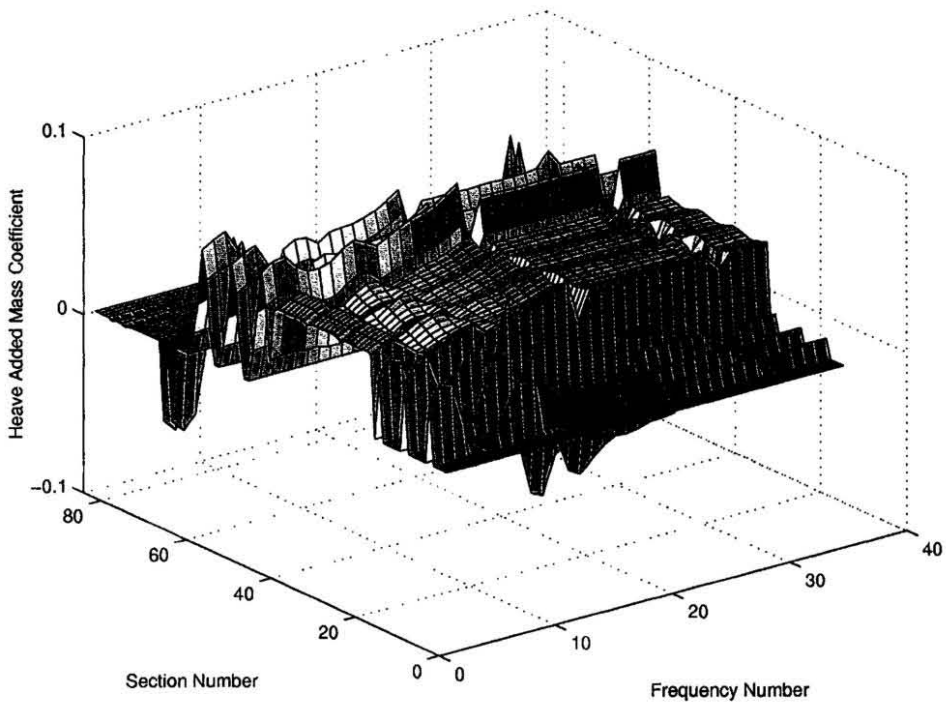

Figure 19: Heave Added Mass versus Frequency and Section Number

The added mass is computed during preprocessing by the routine 3DCOLD. Figure 19 shows a surface plot of heave added mass (A_{33}) versus frequency and section number for the original discretization. Knowledge of the symmetry of the vessel allows

visual inspection of these data for likely inaccuracies. Sections 1-18, 19-43 and 44-63 should be equivalent based on symmetry, however, only the second two ranges showed similar values but they were much lower than those of the first range.

To investigate the source of this discrepancy, a careful examination of the geometric information passed to 3DCOLD was carried out. The panels required for the radiation calculation are generated automatically from the MOTSIM geometry data file using the program PREP3LD.. This routine performs any required rotation or translation of the geometric data and cuts the panels at the calm waterline so that the panels passed to 3DCOLD represent the calm water wetted surface of the vessel. Figure 20 shows the panels generated by this routine for the triangular semi submersible.

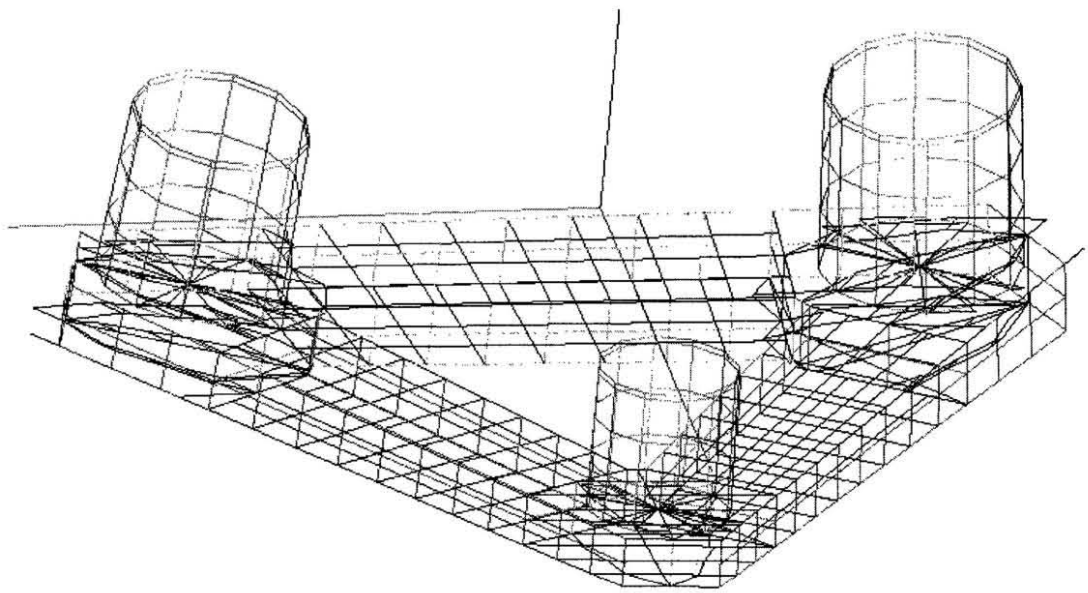

Figure 20: Initial Automatic Panelization for 3DCOLD

It was evident from this figure that the joint regions under the aft main columns were not translated correctly. As it turned out, this error in translation had already been corrected in another version of the PREP3LD code. Figure 21 shows the panel information produced using the updated version. This corrected geometry information was used to recalculate the added mass and damping coefficients using 3DCOLD. Again, the surface plot in Figure 22 indicates the value of A_{33} as a function of section number and frequency. In this plot, the symmetry of the coefficients was as expected given the axi-symmetry of the vessel.

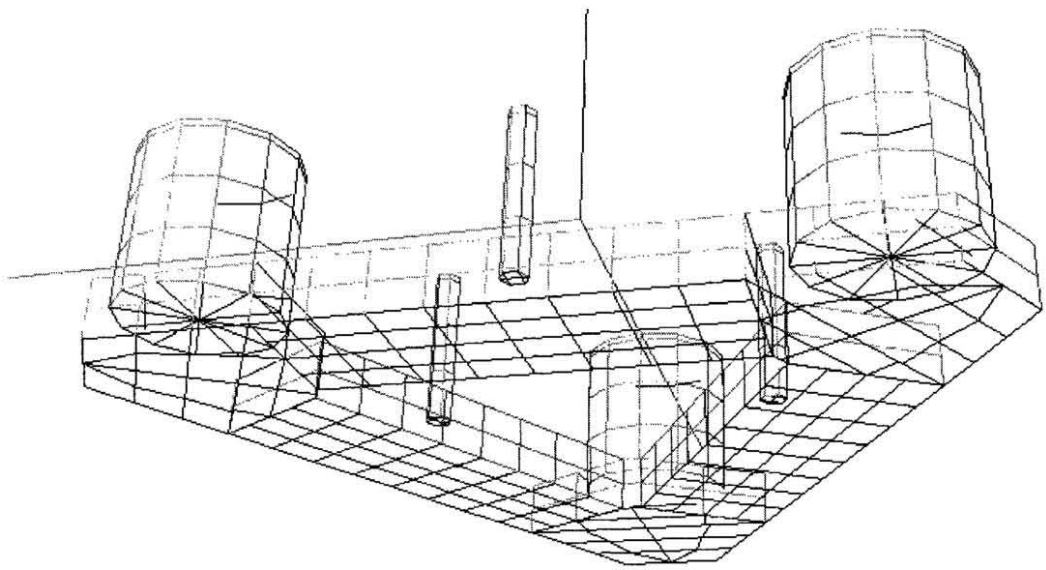

Figure 21: Updated 3DCOLD Discretization

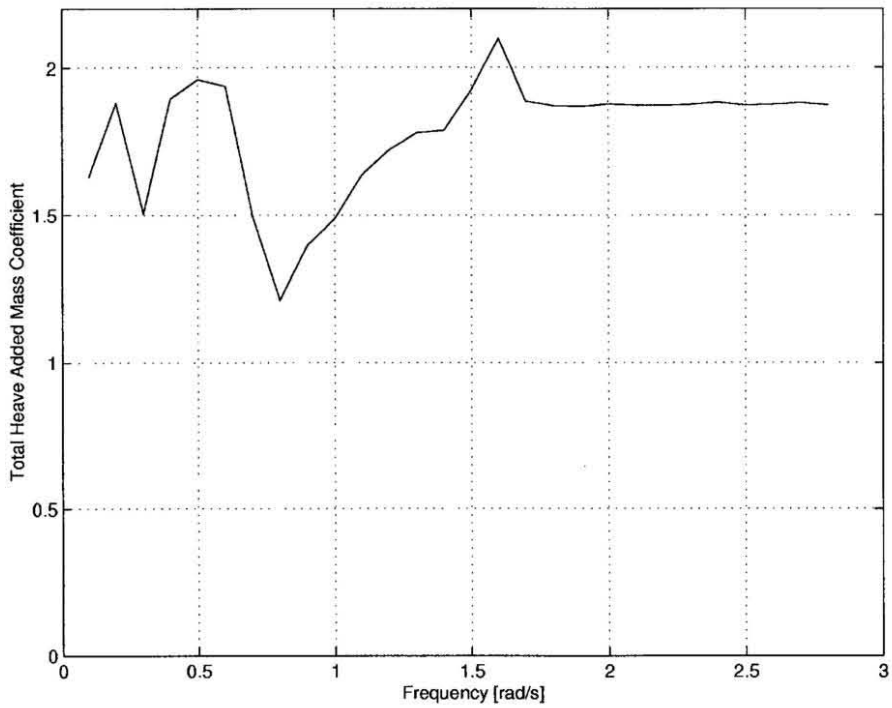

Figure 22: Heave Added Mass vs. Frequency and Section Number for Revised Geometry

The heave decay of the vessel was simulated using the coefficients from the corrected panel geometry and the result is shown as Figure 23. The heave natural period from this simulation was about ten percent higher than that of the model tests, which from Equation 8 indicated that the effective mass had increased too much. Figure 24 shows the total heave added mass A_{33} total as a function of frequency for the unit. The added mass at a frequency of 0.34 (corresponding to T=18.5s) was about 10% higher than the required added mass calculated from Equation 8.

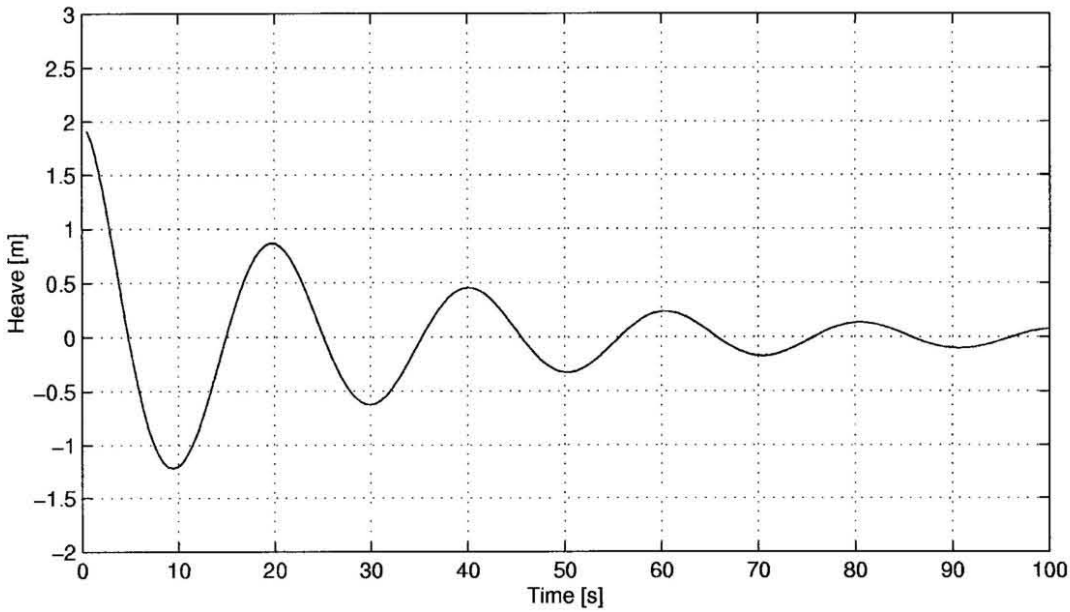

Figure 23: Heave Decay with Corrected Geometric Data

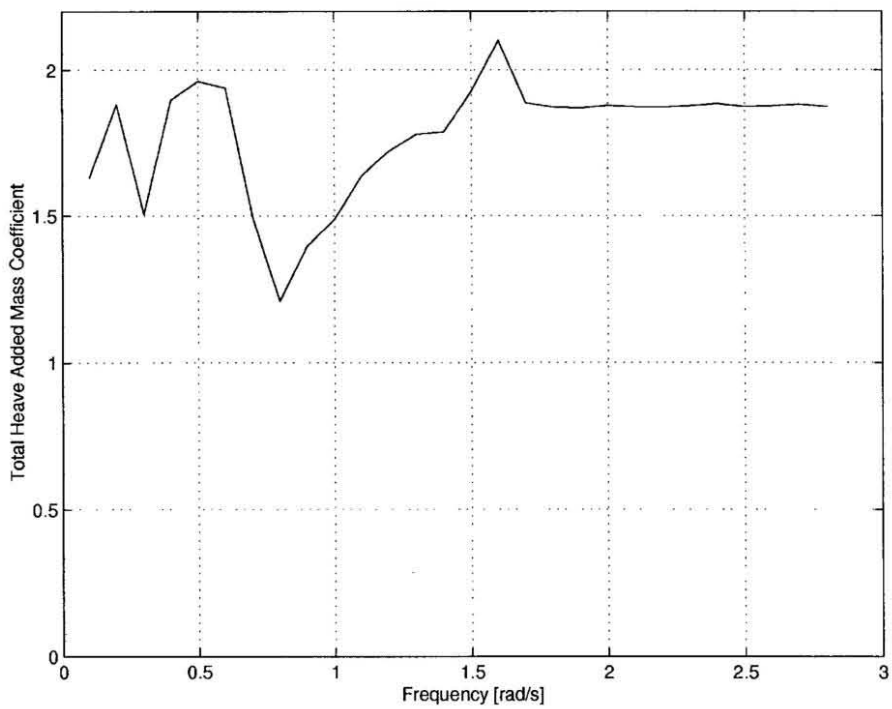

Figure 24: Total Heave Added Mass for Triangular Semi Submersible

Since Figure 23 indicated that the form of the vessel was correctly represented in the panel data file, the effect of the mesh quality and density on the calculated results as well as the accuracy of the radiation solver were investigated. To address this issue, a series of calculations were made for a rectangular box for which results were published in JRME (2000). The box geometry was meshed with four different density and distribution combinations as indicated in Table 1 and shown in Figures 25 through 28. The radiation calculation was repeated over a range of frequencies as described in JRME (2000).

Table 1: Details of Rectangular Box Mesh Variations

Mesh	Number of Divisions			Spacing	Total Panels
	Length	Width	Depth		
A	32	12	10	Cosine	1264
B	32	12	10	Uniform	1264
C	16	6	5	Cosine	316
D	16	6	5	Uniform	316

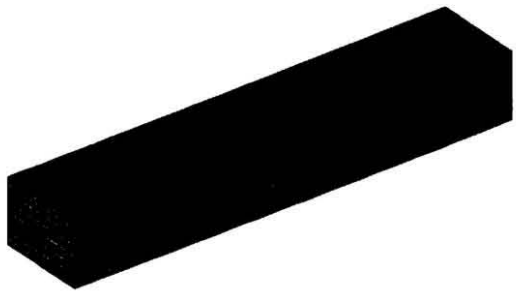

Figure 25: Box Mesh A

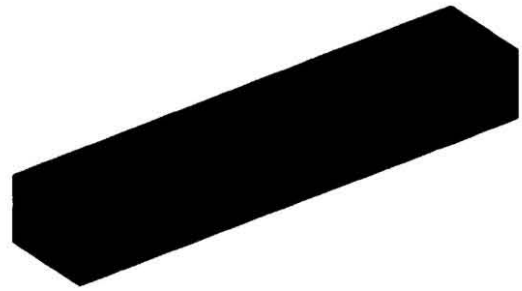

Figure 26: Box Mesh B

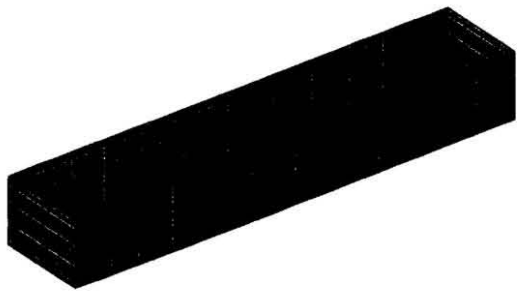

Figure 27: Box Mesh C

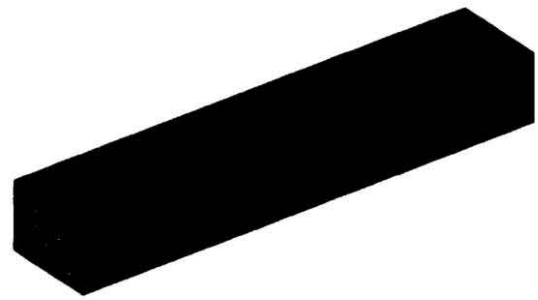

Figure 28: Box Mesh D

Initial results showed poor correlation between the computed and published values. As the program on which this code was based was verified in Sen (1988), an earlier version of the solver was then used to check for errors occurring in recent modifications to the code. Figures 29 to 34 show the added mass coefficients for the six standard motions computed using the earlier version of the radiation solver for each box grid as a function of wave period. Comparison of these results with Figures 35 to 40 reproduced here from JRME (2000) showed good agreement between the radiation solver used here

and those described in the paper and that there was little effect on the solution quality within the range of mesh sizes used.

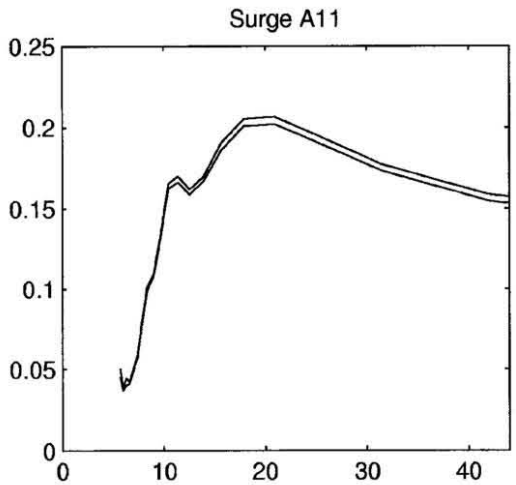

Figure 29: Surge Added Mass Coefficient

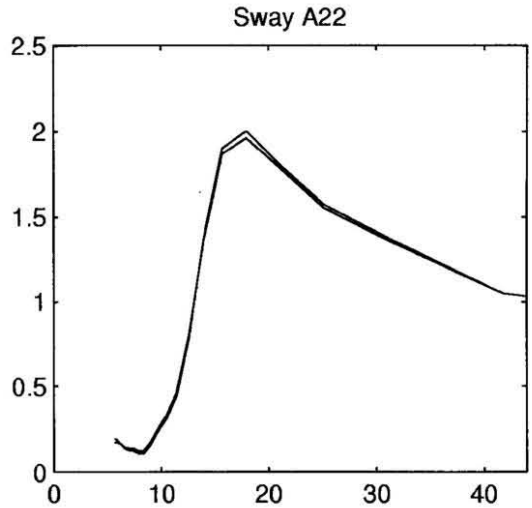

Figure 30: Sway Added Mass Coefficient

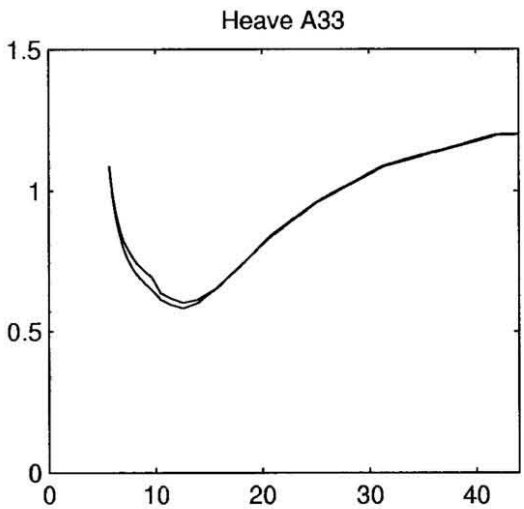

Figure 31: Heave Added Mass Coefficient

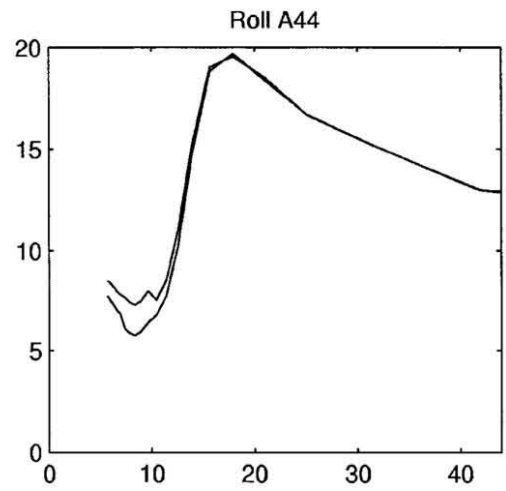

Figure 32: Roll Added Mass Coefficient

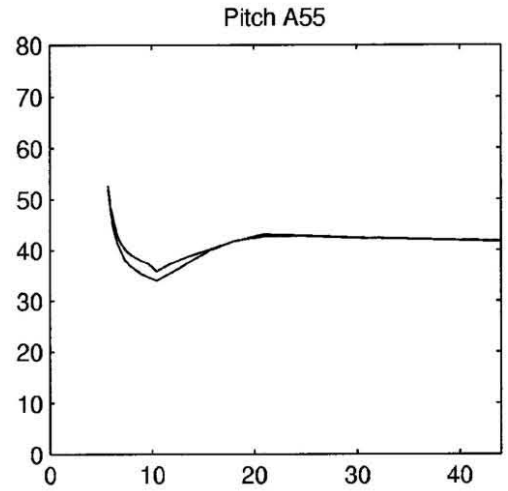

Figure 33: Pitch Added Mass Coefficient

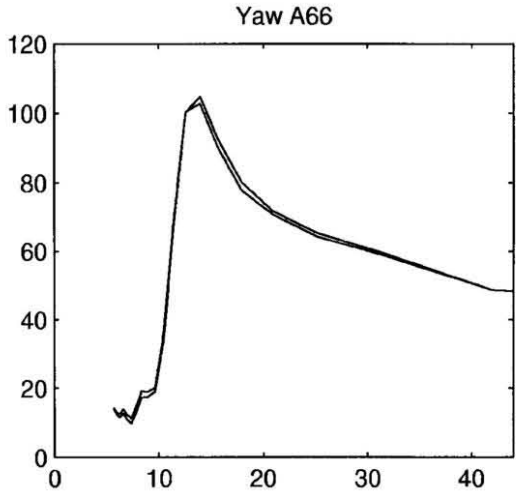

Figure 34: Yaw Added Mass Coefficient

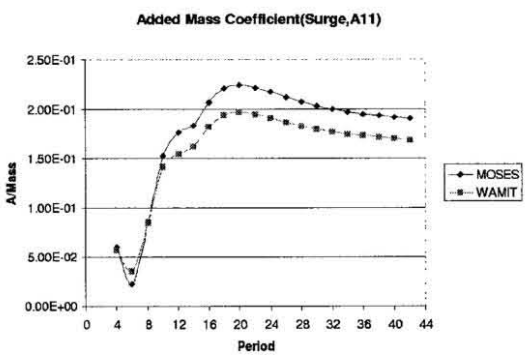

Figure 35: Surge Added Mass Coefficient (JRME)

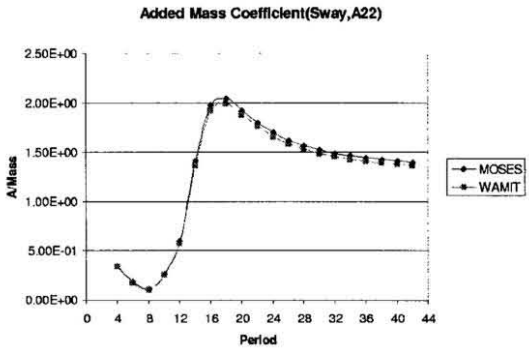

Figure 36: Sway Added Mass Coefficient (JRME)

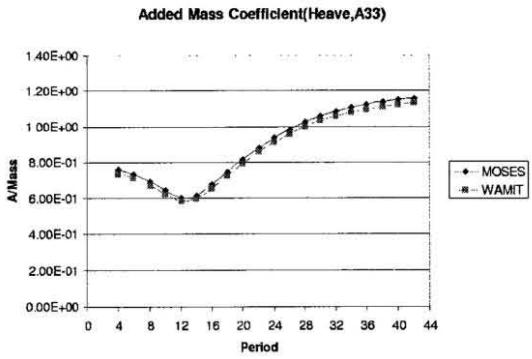

Figure 37: Heave Added Mass Coefficient (JRME)

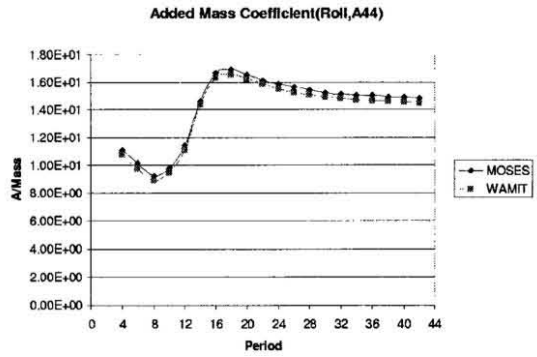

Figure 38: Roll Added Mass Coefficient (JRME)

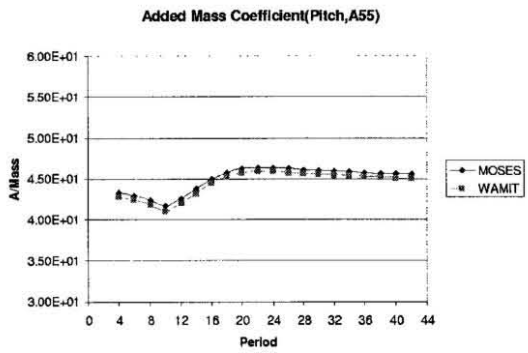

Figure 39: Pitch Added Mass Coefficient (JRME)

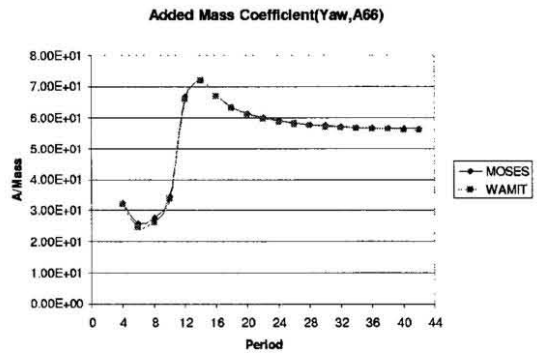

Figure 40: Yaw Added Mass Coefficient (JRME)

In determining the best choice of mesh, it must be noted that there is a significant cost involved in using increased mesh density. Since the radiation calculation requires a number of operations which is proportional to the square of the number of panels, doubling the panel density in each surface direction would quadruple the number of panels and increase the run time by a factor of sixteen. As the time required to complete

this computation for the semi-submersible model was on the order of two hours for the original mesh, the modified mesh could take about 32 hours to compute on the same computer equipment. Clearly a compromise must be made between accuracy and efficiency for the practical application of these methods.

Based on these findings, the corrected panel information was used with the verified version of the radiation solver, however, the results still showed spurious points. At this point, the structure of the panel data was revised again. Panel data for typical panel based radiation solvers must fully enclose the volume of the vessel with panels which do not overlap and whose normals are directed into the fluid domain. Due to the limitations of the MOTSIM geometric format, which made it very difficult to match panels at the interfaces of the components described above, each component was meshed independently with panels of opposite orientation at the interfaces. This simplification was expected to work well for the time-domain solver as the Froude-Krylov and hydrostatic forces on the facing panels would nullify each other thus giving the correct result. To investigate whether this simplification caused the erratic results in the radiation solution, the panels at the interface regions were removed or altered and the solution computed again. The heave added mass coefficient for the modified mesh is presented in Figure 41. Here, the result was much more stable and more consistent with the expected result.

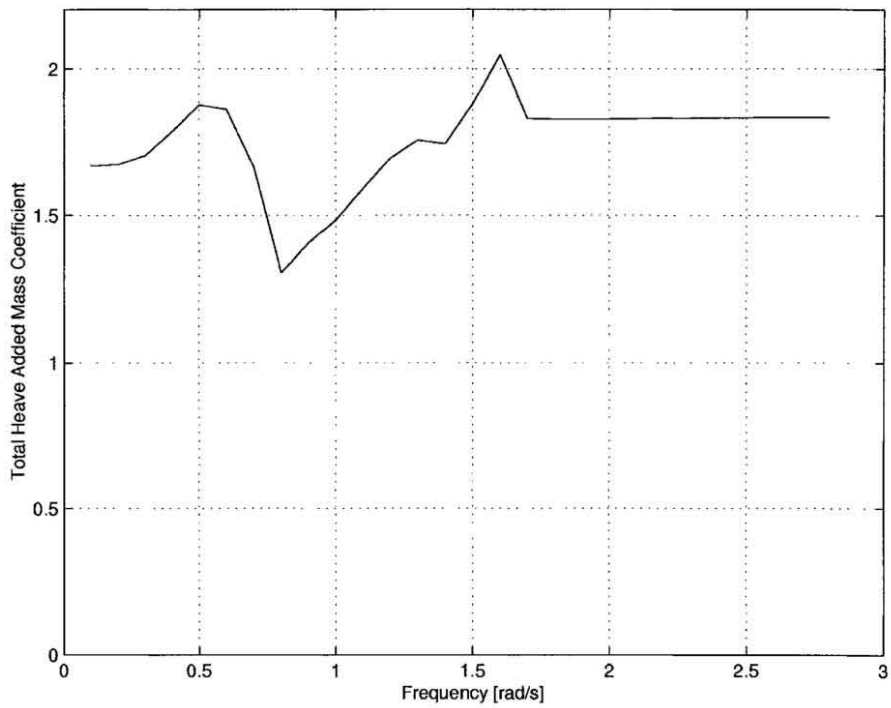

Figure 41: Heave Added Mass with Facing Panels Removed

Heave, roll and pitch decay simulations were performed again using the corrected radiation solution. These results are presented in Figures 42, 43 and 44, respectively. While there was still some variation from the measured results, the correlation was of acceptable quality to proceed with simulations in waves.

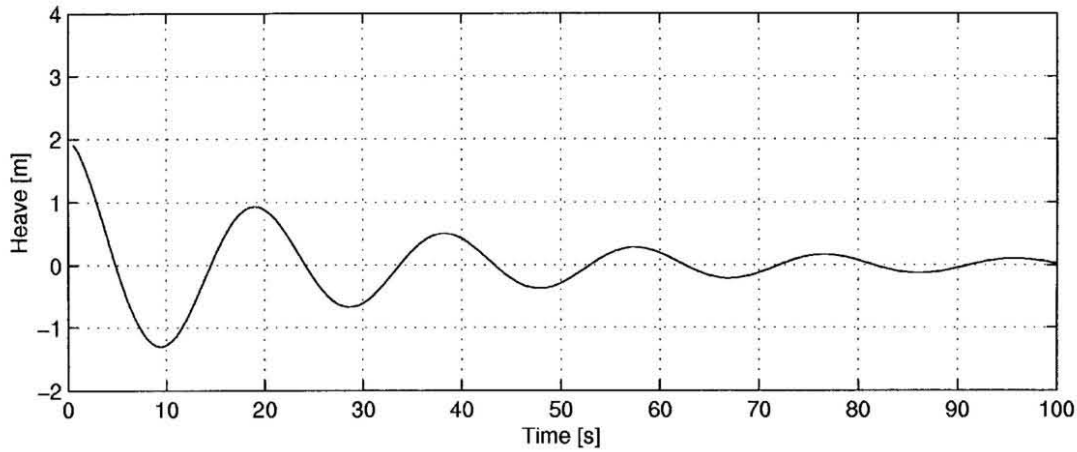

Figure 42: Heave Decay Simulation Results with Corrected Panel Model

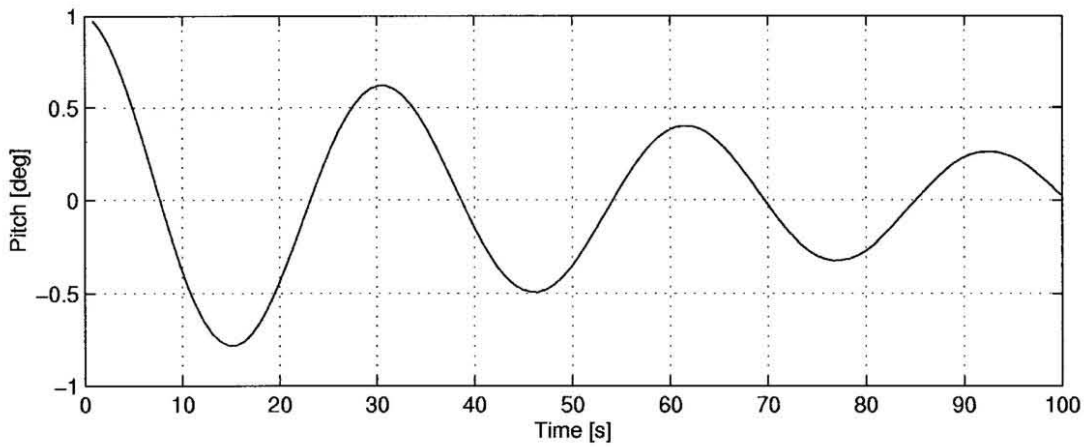

Figure 43: Pitch Decay Simulation Results with Corrected Panel Model

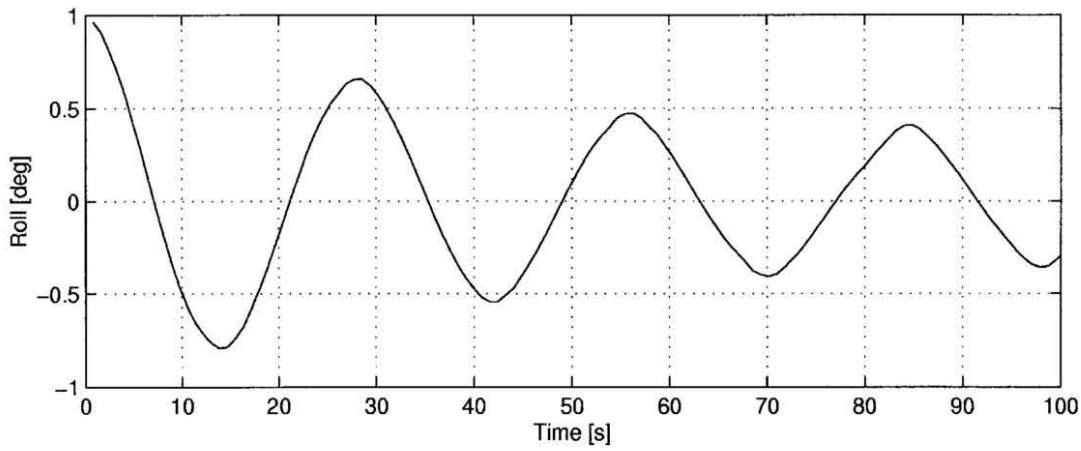

Figure 44: Roll Decay Simulation Results with Corrected Panel Model

4.3.3 Moored Simulations

Consistent with the experimental test program, a compliant spring mooring system was used to restrain the model during the simulations in waves. The mooring was implemented as a subroutine and added to the force summation in MOTSIM. This subroutine allowed specification of the mooring line length, spring constant, attachment position on the vessel and attachment location in the earth-fixed frame.

4.3.3.1 Comparison of Results in Regular Waves

Regular wave tests are typically performed to generate response amplitude operators (RAOs) which can be used to predict vessel response in other wave conditions based on linear superposition. Since many naval architects use numerical seakeeping software tools based on strip theory, regular wave tests are frequently performed to assess the validity of the models they used to develop the design of a vessel. Time domain

simulations were performed for the semi-submersible platform described in the preceding sections to compute RAOs for the motions as recorded in the model tests.

For all the simulations described in this section, the simulation duration was set to be one hundred wave periods. Normally, as few as ten periods can be used to determine the amplitude of vessel motions. The additional time was allowed in this case to permit the startup transient of the spring mooring to dissipate. Figure 45 shows a typical time series of the surge and sway motions of the vessel including the initial transient. A steady motion portion of each simulation was used for the calculation of statistics and RAOs as indicated by the dashed vertical lines in the figure.

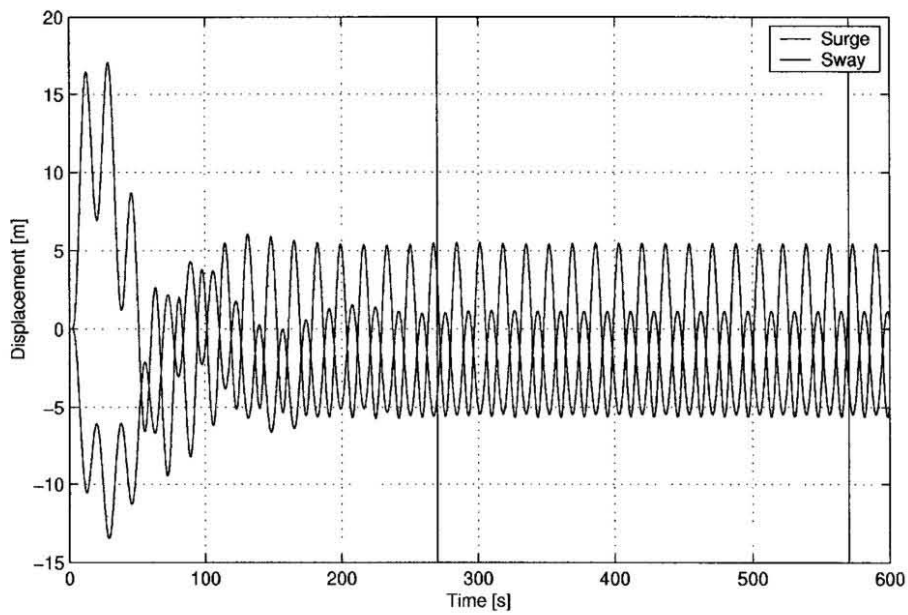

Figure 45: Sample Surge and Sway Time History for Spring Moored Simulation

Response amplitude operators at three wave headings are presented for global x and y direction motions, heave, roll and pitch as Figures 46 through 50, respectively. In general, there is a very good correlation between the experimental and computed RAOs.

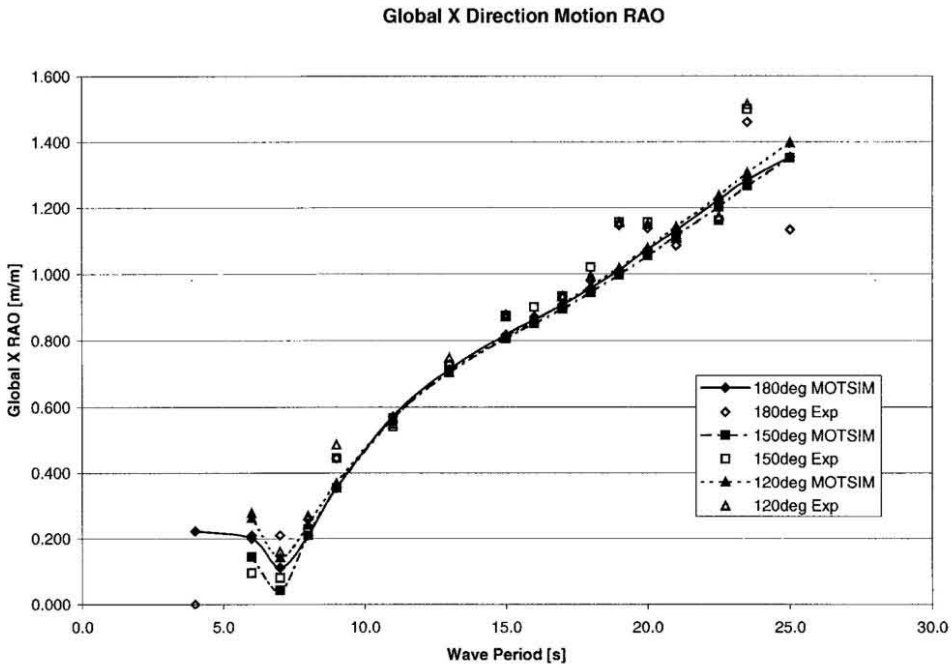

Figure 46: Global X-Direction Motion RAO for Triangular Semi

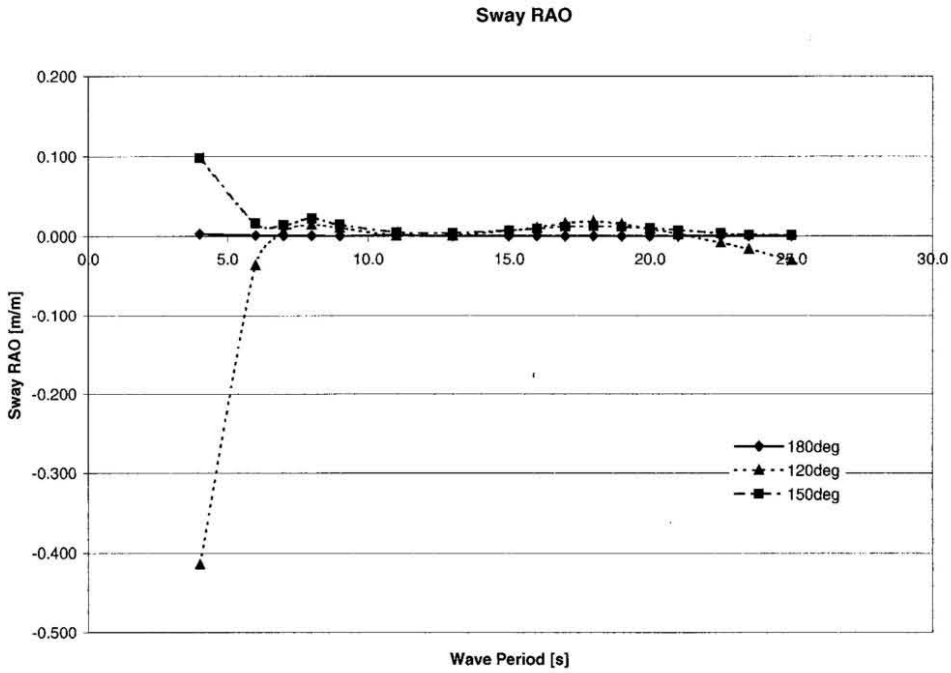

Figure 47: Sway RAO for Triangular Semi

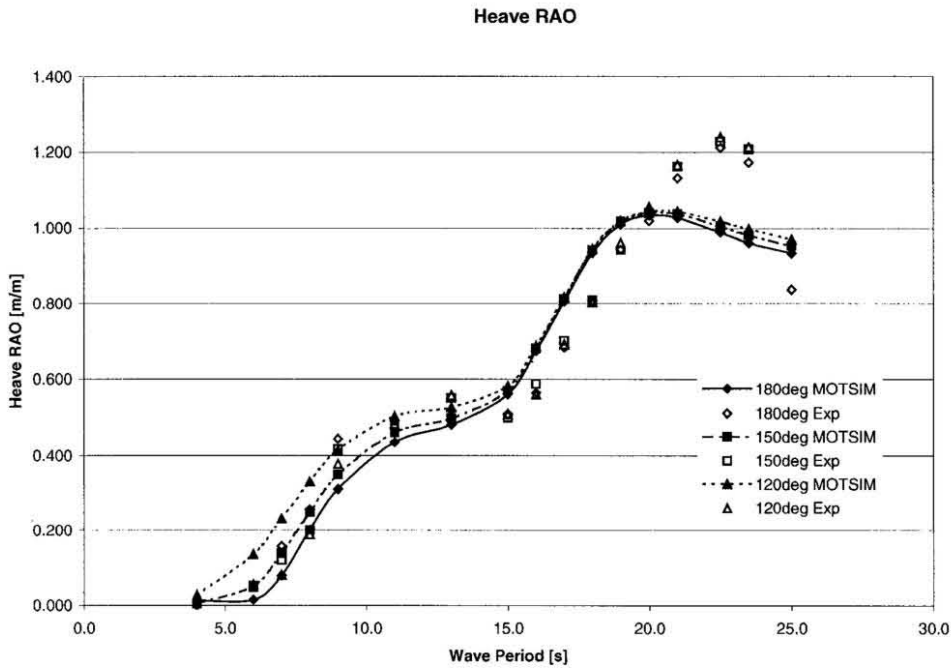

Figure 48: Heave RAO for Triangular Semi

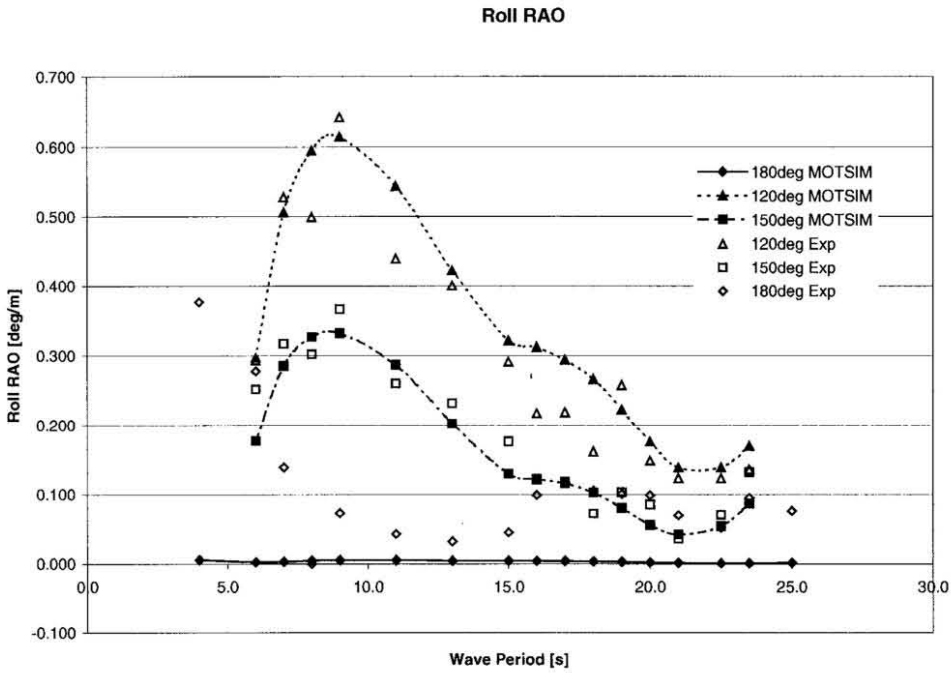

Figure 49: Roll RAO for Triangular Semi

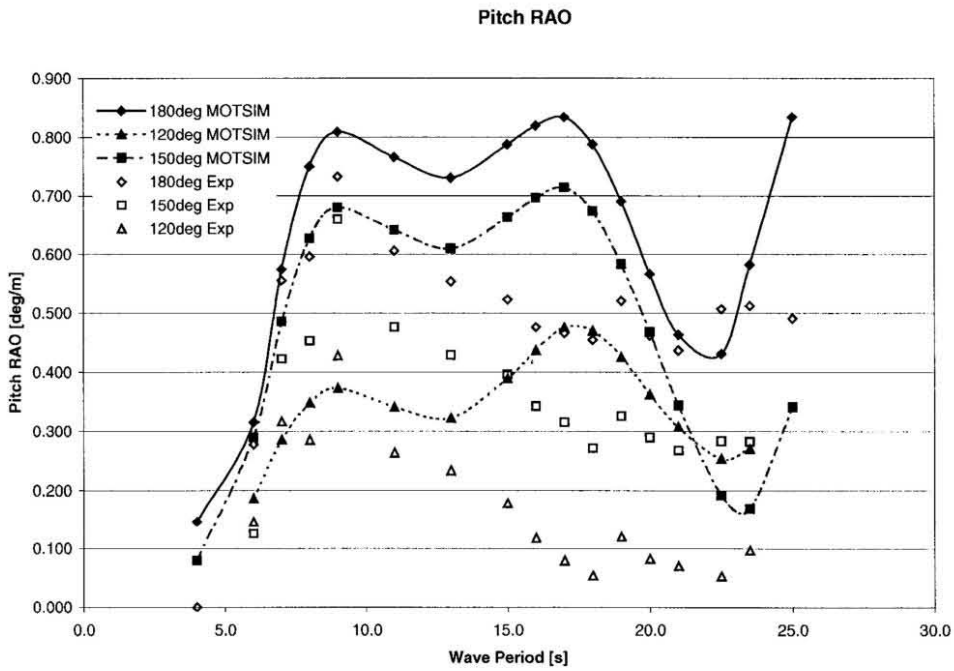

Figure 50: Pitch RAO for Triangular Semi

The global x-direction surge motion indicated very good prediction of the trend over the lower wave periods up to about eighteen seconds. Beyond this period, the experimental results showed some variation which was consistent between wave headings, but was not reproduced by the simulated results. Review of the wave calibration statistics presented in Appendix A of Harris et. al. (1999) indicated that there was more variation in the incident wave height at some of the longer wave periods than at the lower ones. This variation may have contributed to the difference between the computed and experimental results.

The global y-direction sway RAO is presented as Figure 47. This figure shows a significant discrepancy between the predicted and measured results, particularly, the computed results are consistently near zero. Since a unidirectional wave does not provide any exciting force perpendicular to its direction of propagation, this difference is likely attributable to minor asymmetries in the experimental setup or model which are not present in the numerical simulations. Also, eddy shedding off the columns or other portions of the model due to wave particle motion may have contributed to the wave perpendicular excitation. Since the potential flow formulations used by MOTSIM are inviscid, this effect would not be computed.

The heave RAO (Figure 48) again showed generally good correlation with the experimental results and within the data sets for the different wave heading angles. The plateau in the experimental data between wave periods of 8 to 15 seconds, while discernible, is somewhat less distinguished in the simulated results. As for the surge

results, there was some discrepancy between the results at higher wave periods. The computed results showed the peak response of about 1.03 at a period of twenty seconds which is just slightly above the natural heave period of about 18.5 seconds (based on the physical model). The response then decreased slightly below the expected asymptotic value of unity. The experimental values, in contrast, peaked at a value of about 1.2 at a wave period near 22.5 seconds. As discussed in Section 4.3.2.2, this difference may be due to some error in the computation of the heave added mass coefficient at the longer wave periods. It is interesting, however, that the peak response in the experiments is somewhat distant from the reported natural period of the model.

The roll motion RAO shown in Figure 49 again showed reasonably good correlation in the trends and in location and magnitude of the peaks for both 120 and 150 degree wave headings. As discussed in reference to the sway motion, the idealization of the numerical simulation resulted in a roll RAO of zero for the 180 degree heading while the experiment showed small non-zero values at most wave periods. As for most of the motions, the numerical predictions indicated much smoother variations than did the experimental results. Many of the localized variations in the measured results may be thought to be erroneous except for the correlation between the results at different wave headings. Given this repeatability, it is reasonable to assume that these may be due to effects such as viscosity, which were not properly treated by the numerical simulations.

The pitch RAO shown in Figure 50 showed significant differences between the experimental and computed results over the majority of the wave period range. The

correlation between experiment and simulation was fairly good at all wave headings up to about the 13 second wave period. In this range, the experimental peak at a wave period of nine seconds was replicated, though its magnitude was slightly overpredicted, by the simulation. Beyond this wave period range, however, the numerical results indicated a second, larger peak while the measured results trended toward a constant, lower value. As observed for the other motions, the experimental data showed some localized variations above the 18 second period. The most likely contributor to the difference between the results was the vertical location of the mooring lines on the vessel in the numerical simulations. The correct attachment point for the lines is not recorded in the test report, hence, the mooring lines were attached at the vertical position of the centre of gravity as is common practice in tank testing. This convention may not have been used in the experiments, however, because the prototype vessel was intended for moored use and the design fairlead locations would likely have been used.

4.4 Conclusions

The results presented in this chapter indicate that the MOTSIM time-domain seakeeping code is capable of producing reasonable results for a multiple waterplane semi-submersible platform. It was shown that the planned treatment of the body as a group of independently meshed volumes was not suitable for the solution of the radiation potential, rather the traditional method of meshing with non-overlapping panels must be used. Particular care must be taken in the meshing of these small waterplane vessels since small errors in displaced volume, normally acceptable for a displacement vessel, result in unacceptable variations in draft and forces related to waterplane area.

Chapter 5

Time Domain Simulation of an Articulated Tug Barge (ATB)

5.1 Introduction

An Articulated Tug Barge (ATB) is a tug and barge combination in which the two vessels are connected rigidly in some directions and compliantly in others. One of the most common methods for connecting the tug to the barge is with the Intercon® system. This patented system features a pair of electrically actuated pins installed on either side of the tug. These pins extend into fittings on the inner faces of a notch in the stern of the barge and allow for relative motion in pitch while restraining all other relative motions. Other interconnection systems feature yoke type connections which allow heave and pitch relative motion or fully constrained systems (called Integrated Tug Barge or ITB). A typical ATB unit is shown as Figure 51.

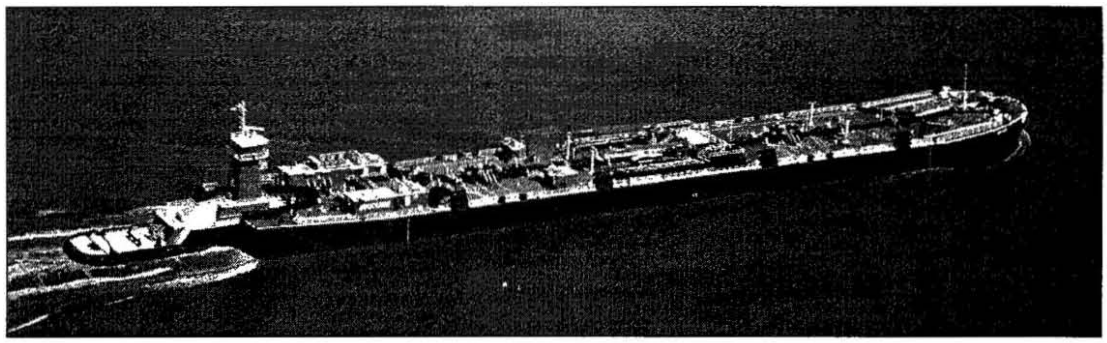

Figure 51: Photograph of a Typical Articulated Tug Barge Unit

ATB units are very popular in the North American domestic shipping market for a number of reasons, not the least of which is a loophole in the United States Governmental regulations which places fewer restrictions on these vessels as compared to a traditional ship of similar size. The Jones Act treats the components of an ATB as a small tug and an unmanned barge. These components are hence subject to fewer regulations than a similarly sized conventional ship (Marine Log, 2000). Among the differences, a much smaller crew is required to man the ATB, thus resulting in significant life cycle cost reductions. Modern ATB units are used to transport everything from rail cars and truck trailers to oil and other liquid chemicals. By necessity, the primary pilot station on the tug of an ATB is typically high above the water surface (as seen in Figure 51) causing the accelerations experienced by the pilot to be amplified beyond those experienced at deck level.

Owing to the popularity of ATB's and the perceived market for computational analysis of multiple vessel seakeeping, a new version of the MOTSIM seakeeping code was developed to permit simulation of two vessels simultaneously with or without

mechanical interaction forces between them. In the present validation study, a set of rigid constraints was used to simulate the effects of the pinned joints in the ATB unit and to allow computation of the connection loads at the pins.

Oceanic Consulting Corporation of St. John's, Newfoundland has conducted model scale experiments on several pinned ATB units over the past several years. The results from one of these studies were used here to validate the constrained multiple vessel version of MOTSIM. The physical model test program included tests in head seas with forward speed and zero speed tests at oblique wave headings. The tests without forward speed were conducted while the model was moored using a compliant spring mooring system. It should be noted that, in the interest of client confidentiality, vessel particulars and dimensional values are omitted in this document. In this chapter, the results of that study are compared to those computed by the multiple vessel MOTSIM seakeeping simulation software package to assess the suitability of the software for the characterization of tandem multiple vessel systems.

5.2 Modifications to MOTSIM

To facilitate the simulation of an ATB, substantial modifications were required to the MOTSIM code. First, the code was modified to permit simulation of multiple floating bodies using the same executable file. Second, an algorithm was developed and implemented to permit simulation of the pinned joint between the vessels. These modifications were performed under the author's technical direction and supervision, however, much of the actual programming required was performed by other employees

of Marineering Limited. The details of these modifications are described in the following sections.

5.2.1 Extension to Two Vessels

Extending MOTSIM's capabilities to allow simulation of two vessels required that essentially two copies of the code be run simultaneously whilst maintaining coupling between the simulations at each time step. A number of schemes were considered for the implementation of the multibody MOTSIM. Initially, a supervisory program which would run two copies of the standard MOTSIM and perform coupling through file input and output was considered. This option was proposed as it appeared to be the simplest to implement, however, it was deemed to be extremely inefficient and limited in its adaptability for coupling forces. A parallel processing model was also considered which would use a message passing library such as PVM (Dongarra et.al., 1997) to manage the execution of the code on multiple processors while inter-vessel coupling was handled by a master program. This option was discarded due to the estimated level of effort required to learn and implement the parallel processing libraries versus the savings over sequential execution. Finally, a model was selected whereby two sets of MOTSIM subroutines are executed sequentially to compute the forces acting on the individual vessels and the resulting two body system is integrated using a single solver. This allows complete flexibility in the coupling of the bodies.

The implementation of the two body MOTSIM can best be understood by first considering the single vessel version's general execution flow. The solution is advanced

in time by the routine DRIVE which calls FORCE to compute all forces acting on the vessel at that instant. The net force on the body comprises Froude-Krylov and diffraction forces along with contributions from additional models such as propulsion, steering, moorings etc. The forces are used with the past state of the system and the inertial matrix to define the equations of motion as a system of twenty-one linear differential equations (this includes solution of additional models such as roll tanks) which are then solved using an Adams-Bashforth-Moulton Predictor-Corrector scheme (Bass, 1988).

The two-vessel version is modified such that the BIGDRIVE routine calls BIGFORCE to determine all forces in the system. BIGFORCE subsequently calls FORCE and NFORCE to compute the forces for the first and second vessels respectively. Additional interaction forces can be added to the system in this routine (as will be described in the following section). These forces are used by BIGDRIVE to define a system of forty-two linear differential equations for the motion of both vessels.

Without addition of constraining forces, the resulting program functions like two independent copies of MOTSIM except for the time stepping and solution of the equations of motion. This fact allowed the modified version of the code to be validated against simulations with the original version of MOTSIM.

It should be noted here that the intent of these modifications was only to provide a software framework for continued development of a simulation tool capable of simulating the dynamics of multiple floating bodies. No effort has been made at this time to model the hydrodynamic interaction between the bodies. This simplification is

anticipated to provide reasonable results for the ATB since the vessels are aligned end to end hence the region of interaction is reasonably small compared to other possible configurations such as side-by-side vessels.

5.2.2 Constraint Modeling

As described above, the tug and barge of an ATB system is coupled by a pair of collinear pins which form a joint allowing only relative pitch motion between the vessels while forming a rigid coupling in all other modes of motion. In MOTSIM, a holonomic constraint is used to model the effects of this joint between the vessels.

5.2.2.1 Mathematical Basis

If the positions and orientations of the two vessels are specified by a vector $\vec{r}$, where the components of $\vec{r}$ are the Cartesian coordinates plus Euler angles of both vessels, i.e.,

$$\vec{r} = (x_1, y_1, z_1, \alpha_1, \beta_1, \gamma_1, x_2, y_2, z_2, \alpha_2, \beta_2, \gamma_2) \tag{13}$$

A holonomic constraint (Saletan & Cromer, 1971) is defined by a relation of the form

$$g(x_1, y_1, z_1, \alpha_1, \beta_1, \gamma_1, x_2, y_2, z_2, \alpha_2, \beta_2, \gamma_2) = 0. \tag{14}$$

Applying the constraint restricts the solution $\vec{r}$ to lie on surface g in the coordinate space. A number of constraining relations of the form (14) may be applied at one time. The solution would then lie on the intersection of the surfaces. The total number of constraints must be fewer than the dimensions of the coordinate space, in this case twelve.

The equations of motion for the system are given by

$$M\frac{d^2\vec{r}}{dt^2} = \vec{F} = \vec{F}_{ext} + \vec{F}_{cons}, \tag{15}$$

where M is the inertial mass matrix for the two vessels, $\vec{F}_{ext}$ contains the external forces and moments, and $\vec{F}_{cons}$ is the constraining force vector. In the no friction limit, each constraint contributes only the force required to keep the system on the defining surface g. Thus the direction of the constraining force is normal to surface g, and may be expressed by (Saletan & Cromer, 1971):

$$\vec{F}_{cons} = \lambda(t)\nabla g, \tag{16}$$

where λ is a scalar, and is known as a Lagrange multiplier (Edwards & Penney, 1990). Substituting (16) in (15) gives

$$\vec{F} = \vec{F}_{ext} + \sum_{i=1}^{I} \lambda(t)_i \nabla g_i, \tag{17}$$

where I is the number of constraints applied.

Since the solution $\vec{r}$ lies along the surfaces g, the velocity vector will be perpendicular to these surfaces. This is expressed by d'Alembert's principle (Saletan & Cromer, 1971)

$$\nabla g_i \bullet \vec{v} = 0, \qquad i = (1..I), \tag{18}$$

where $\vec{v}$ is the velocity vector. Equations (17) and (18) are solved to determine $\vec{r}$ and the Lagrange multipliers.

To facilitate the solution of these equations, Equation (18) was differentiated with respect to time, then simplified to give:

$$\nabla g_i \bullet M^{-1} \vec{F} = -\left(\vec{v} \bullet \nabla^2 g_i \bullet \vec{v} \right), \qquad i = (1..I) \qquad (19)$$

In the case of the two vessel problem, Equation (19) represents a set of I linear equations in the 12 coordinates and Equation (17) represents a set of 12 linear equations with $12+I$ unknowns, i.e. the 12 force components plus the I Lagrange multipliers. Combining these sets yields a system of $12+I$ linear equations in $12+I$ unknowns. These are solved in the new BIGFORCE routine by calling LSARG, an iterative method for solving linear systems of equations included in the IMSL Fortran library (IMSL).

Early tests of the software with simple restraints indicated that the solution would drift significantly over time such that the constraints were violated. This resulted in large constraint forces and numerical instability. To overcome this, a correction step was added whereby the predicted vessel positions were corrected by moving the constraint positions back into compliance with the constraint definitions. This correction was computed by projecting the predicted solution back onto the constraint surface using a mathmatical formulation analogous to the original constraint formulation.

5.2.2.2 *The ATB Pinned Joint*

As indicated above, the two-vessel seakeeping problem has twelve degrees of freedom. Since the pinned joint of an ATB allows relative motion in only one degree of freedom (i.e. pitch) it must constrain the motion in the remaining five degrees. Hence, five holonomic constraints were required resulting in a set of seventeen differential equations to solve. This was simplified, however, by using MOTSIM's built-in constraints to reduce the problem to one of motion in the *XZ* plane only. In this situation, only two constraints were required (heave and surge). This requirement was satisfied by implementing a ball and socket type joint between the vessels. The equations for this constraint are developed below.

A ball and socket joint constrains a point on each vessel to be collocated at all times in the global frame with the corresponding location on the other vessel, i.e. to have zero distance between the two points in the global coordinate system. This can be written as:

$$\begin{aligned} f &= x_1 - x_2 = 0 \\ g &= y_1 - y_2 = 0 \\ h &= z_1 - z_2 = 0 \end{aligned} \tag{20}$$

where *f*, *g* & *h* are holonomic constraints in coordinates x, y and z, respectively. In MOTSIM, the instantaneous location of a point is determined from the location of the vessel centre of gravity and the instantaneous rotation matrix as follows:

$$\vec{x}_g = \vec{x}_{CG} + R \cdot \vec{x}_l \tag{21}$$

where *R* is the rotation matrix defined as:

$$R = \begin{bmatrix} \cos\theta\cos\psi & \sin\phi\sin\theta\cos\psi - \cos\phi\sin\psi & \cos\phi\sin\theta\cos\psi + \sin\phi\sin\psi \\ \cos\theta\sin\psi & \sin\phi\sin\theta\sin\psi + \cos\phi\cos\psi & \cos\phi\sin\theta\sin\psi - \sin\phi\cos\psi \\ -\sin\theta & \sin\phi\cos\theta & \cos\phi\cos\theta \end{bmatrix} \quad (22)$$

where φ, θ and ψ represent the roll, pitch and yaw of the vessel.

As indicated in the previous section, the constraint equations (20) had to be differentiated twice with respect to time. To help ensure accuracy, the Symbolic Toolbox in Matlab® was used to perform these manipulations. The resulting equations were included in the BIGFORCE routine to calculate the connection forces.

5.3 Model Tests

5.3.1 Introduction

Oceanic Consulting Corporation designed and constructed a scale model of the concept ATB unit. This model was used in seakeeping experiments conducted in the Ocean Engineering Basin (OEB) and the 200m Clearwater Towing Tank at the National Research Council of Canada's (NRC) Institute for Marine Dynamics (IMD). The details of the relevant portions of the experimental program are described below.

5.3.2 Model

The model was constructed at a scale of 1:25.4. This relatively large scale was selected to permit the outfit of the tug propulsion system. The model consisted of two separate hull models which were coupled during the tests using two purpose-built pin dynamometers. The barge hull model featured a plywood box structure wrapped in Styrofoam™ which was milled to the correct shape then fiberglassed and finished. The

tug model was constructed similarly with the exception that there was no internal box structure included.

5.3.3 Test Facilities and Instrumentation

5.3.3.1 200m Clearwater Towing Tank

Seakeeping tests in head and following waves were conducted in the 200 m Clearwater Towing Tank at IMD. This tank measures 200 m long, 12 m wide by 7 m deep. It features an articulated flap type wave maker at one end and a parabolic beach at the other. This system can generate waves up to approximately one meter in height. The main carriage is capable of speeds up to 10 m/s. A schematic of this tank is shown in Figure 52.

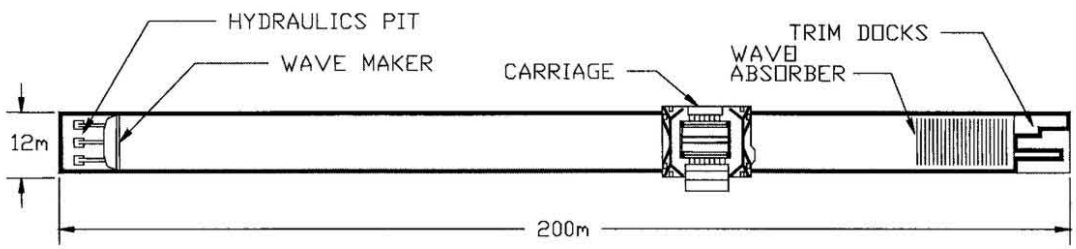

Figure 52: Schematic of IMD 200 m Clearwater Towing Tank

5.3.3.2 Motion Measurement

Motion of the barge model was recorded in six degrees of freedom using Qualysis (described in Chapter 4). The relative pitch motion between the tug and barge was measured using a yo-yo potentiometer. This device provides an output signal which is proportional to the length of wire pulled from it. In the present case, the instrument was installed on the deck of the barge and the wire was attached to a point on the tug above

the pivot location such that pitch motion would cause the length of wire to vary. The linear measurement was converted to an angular value during the analysis.

5.3.4 Seakeeping Experiments

Transit seakeeping experiments were conducted in the 200 m towing basin using a self-propelled model. Tests were performed in two wave spectra and at three speeds. These experiments were performed by accelerating the model in waves using a system of ropes and then releasing it under its own power. The carriage speed was adjusted to follow the model.

The model was restrained in roll, yaw and sway by two guide wires on each side of the model. Four posts located on the model, fore and aft on the port and starboard sides, aligned the model inside the guide wires. For head seas the model was accelerated towards the wave board and for following seas experiments it traveled away from the wave maker. At the opposite end of the basin the model was again restrained using the ropes. The propeller speed was adjusted to maintain target speed prior to beginning the test but was not altered during the tests. When it was not possible to get the full wave train duration in the length of the basin, the wave train was split into segments and additional tests were conducted on each wave segment until the whole wave time series was completed.

5.4 Numerical Simulations

5.4.1 Model Preparation

5.4.1.1 Geometry

The forms of the tug and barge of the ATB unit were converted to the MOTSIM geometric format. Both vessels were represented up to the main deck level as the motions were not expected to be extreme enough to require the superstructure to be included. The tug and barge meshes used for the simulations are shown in Figures 53 and 54, respectively. In the notch region of the barge model, a deck of zero thickness was included to allow the stations to be represented symmetrically with an origin at y=0. This will not result in any error in the code since these panels are excluded from the diffraction calculations and will cancel each other in the case of the Froude-Krylov pressure integration.

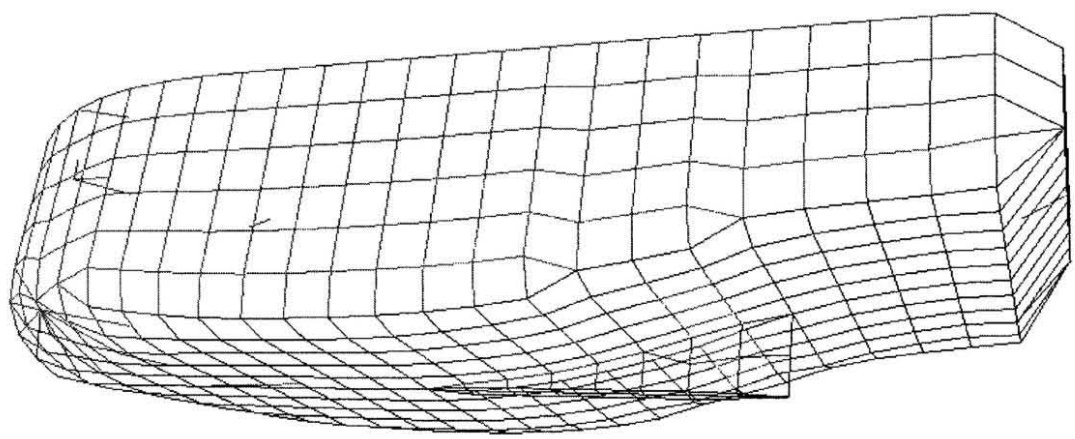

Figure 53: MOTSIM Panelization for Tug

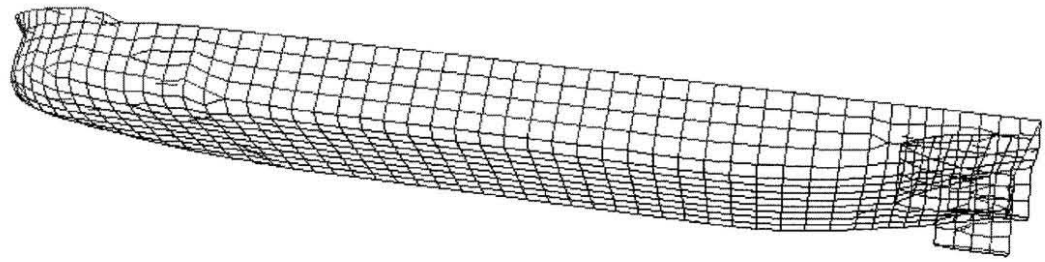

Figure 54: MOTSIM Panelization for Barge

5.4.1.2 Preprocessing

Added mass and damping coefficients were computed for the model using MOTSIM's three-dimensional radiation solver, 3DCOLD. These coefficients were evaluated at twenty-five frequencies. The added mass and damping coefficients were then converted to memory function form for use by MOTSIM.

5.4.2 Verification

5.4.2.1 Hydrostatics

To confirm the quality of the discretized model geometry, the MOTSIM solver was used to compute standard hydrostatic quantities for the vessel for comparison to those obtained by other calculations and through model test measurements. The computed displacement for both vessels were approximately three percent lower than the target which is typical for the type of discretization used. The transverse metacentric height was calculated for the barge and was within one percent of the tested value.

Unlike the tests for the semi-submersible described in the previous chapter, no decay tests were documented for this model test program, so no model verification on this basis was possible.

5.4.3 Simulation Results

A series of simulations were performed in regular and irregular waves for the ATB unit constrained by the ball and socket joint as described above. The initial series of simulations were carried out using a full-scale model of the unit. At this scale, however, the constraint matrix defined by Equations (17) and (19) was ill conditioned and the solution of the Lagrange multipliers was very unstable. This was likely due to the large difference in size between the two vessels. The barge had a displacement of almost fifteen times that of the tug. Also, the distance between the centre of gravity and the pin location is approximately twelve times larger on the barge than for the tug.

Since masses and force scale by the cube of the scale factor while linear distances are scaled directly, it was thought that using model scale data would likely improve the conditioning of the constraint matrix. Hence, all input data was re-scaled to model scale as used in the experimental program. As anticipated, this modification did result in a better conditioned constraint matrix and better stability in the simulation code.

5.4.3.1 Regular Waves

A number of regular wave simulations were performed using the re-scaled geometric data because these were thought to be more easily interpreted than irregular wave simulations as were used in the model test program. Five wave frequencies were

simulated for the ATB at each of three forward speeds. All simulations were performed in head seas. Figures 54 through 57 present time histories of the heave, pitch and resultant connection force (23) for both the tug and barge.

$$F_{res} = \sqrt{F_x^{\,2} + F_z^{\,2}} \tag{23}$$

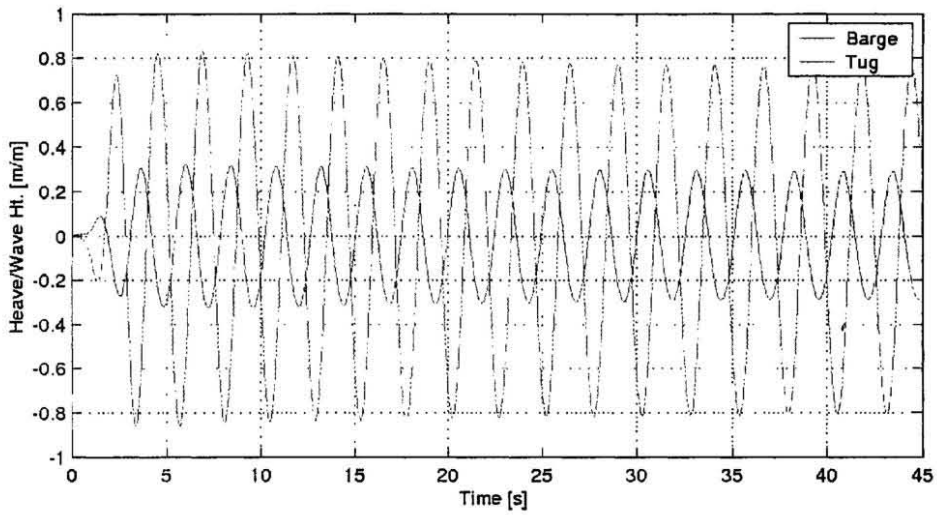

Figure 55: ATB Heave Motion in a Regular Head Wave

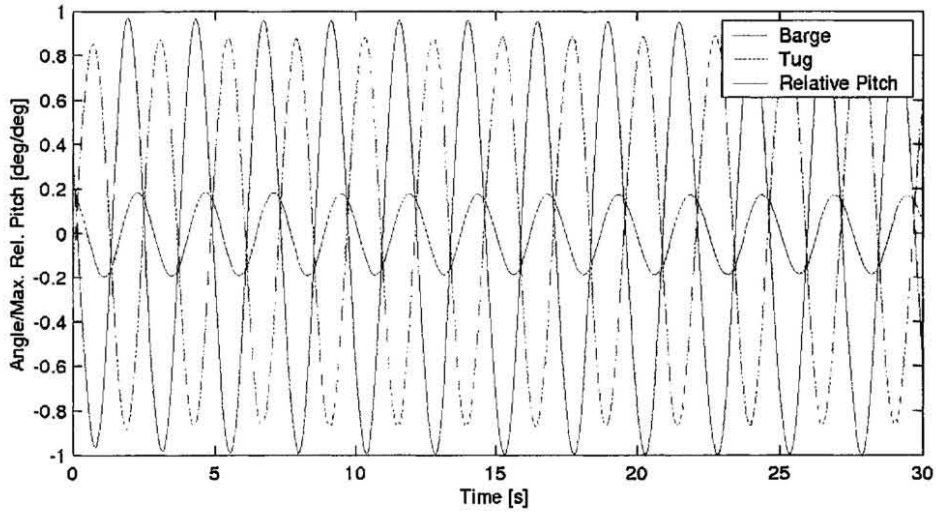

Figure 56: ATB Pitch & Relative Pitch Motion in a Regular Head Wave

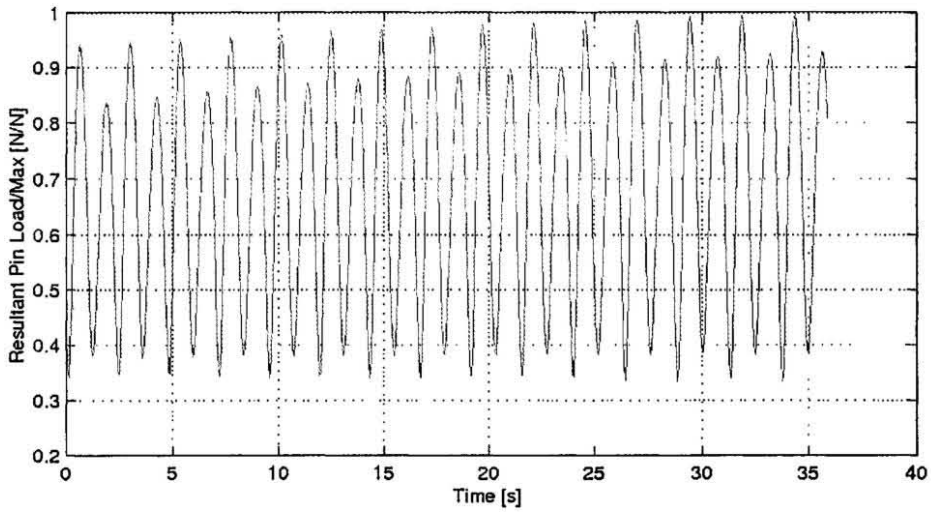

Figure 57: ATB Pin Connection Load in a Regular Head Wave

The regular wave results shown above gave confidence that the constraint model was properly constraining the vessels and was reasonably stable over a sufficient simulation duration. As Figure 57 showed, however, there was some drift in the constraint which

was expected to pose difficulties in longer simulations. Since no regular wave tests were performed for the model, however, it was necessary to continue with irregular wave simulations.

5.4.3.2 Irregular Wave Simulations

The experimental program included head and following wave transit tests in two irregular JONSWAP wave spectra at three forward speeds. Due to time constraints, it was only possible to complete simulations for the head sea case with one wave spectrum. The larger of the two wave conditions was selected.

For transit simulations (or model tests) in a seaway, a full-scale duration of twenty minutes is required. At the model scale of 25.4, this was approximately four minutes. The MOTSIM simulations were setup to run for this duration, however, all simulations failed after about 1.5 minutes of model scale duration. The failure in the simulations was due to instability in the constraint model. Investigation of this in the literature indicated that many methods of rigid body constraint stabilization existed (Ascher et.al., 1994). Because it was unclear whether any particular method would necessarily work better than the projection method already employed no additional efforts were made to stabilize the constraints. Hence, the stable portion of the simulations was analyzed for comparison with the experiments.

Figure 58 shows the normalized RAO for relative pitch between the tug and barge. This RAO is calculated as the ratio of the standard deviations of the pitch motion and the wave height and was normalized by the maximum experimental value to obscure the

actual values. These results indicated that the values from the MOTSIM simulations were slightly below the range of the experimental data. As can be seen in Figure 58, there was significant scatter in the experimental values which may indicate variation in wave quality or measurement consistency. The difference between the results, however, is more likely due to the lack of detailed mass distribution data for the tug. This information was omitted from the documentation of the experiments, hence typical values were used which may not have adequately modeled the actual properties of the tug model.

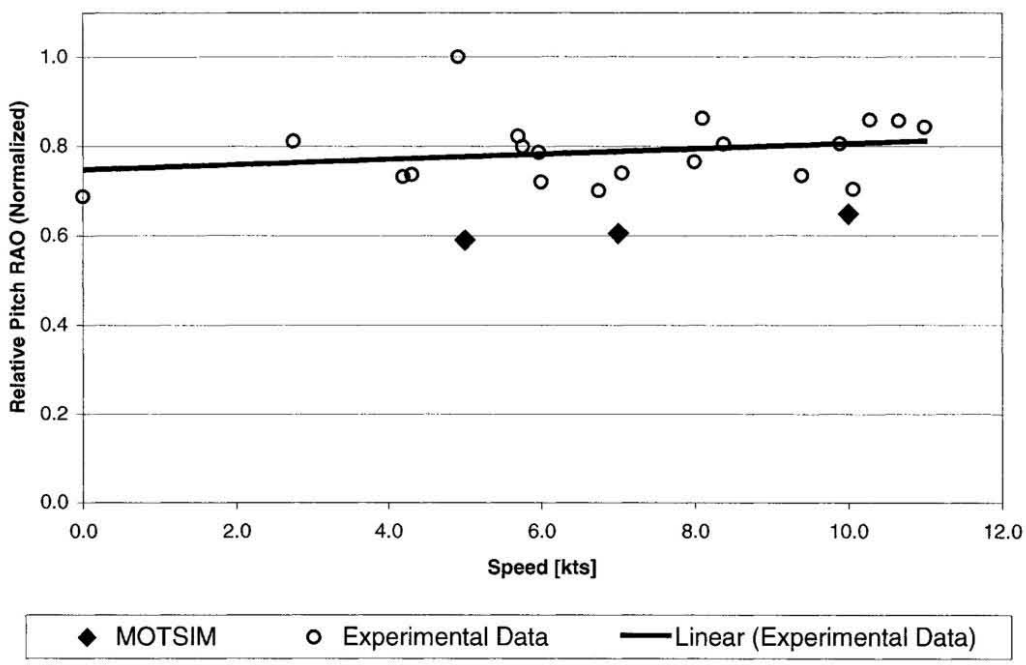

Figure 58: Comparison of Relative Pitch RAO vs. Speed for ATB in Head Seas

Figure 59 presents results for the resultant pin connection force. These data were calculated as the standard deviation of the resultant force (23) normalized by the

maximum value and were plotted against the standard deviation of the wave height. The MOTSIM constraint force was divided in half to represent the load on a single pin. Results for all three speeds fell within the range of the experimental data, but were on the upper bounds for the given wave height. Unfortunately, all simulations used the same wave conditions and hence did not indicate any trend so further simulations are required to validate the force calculations.

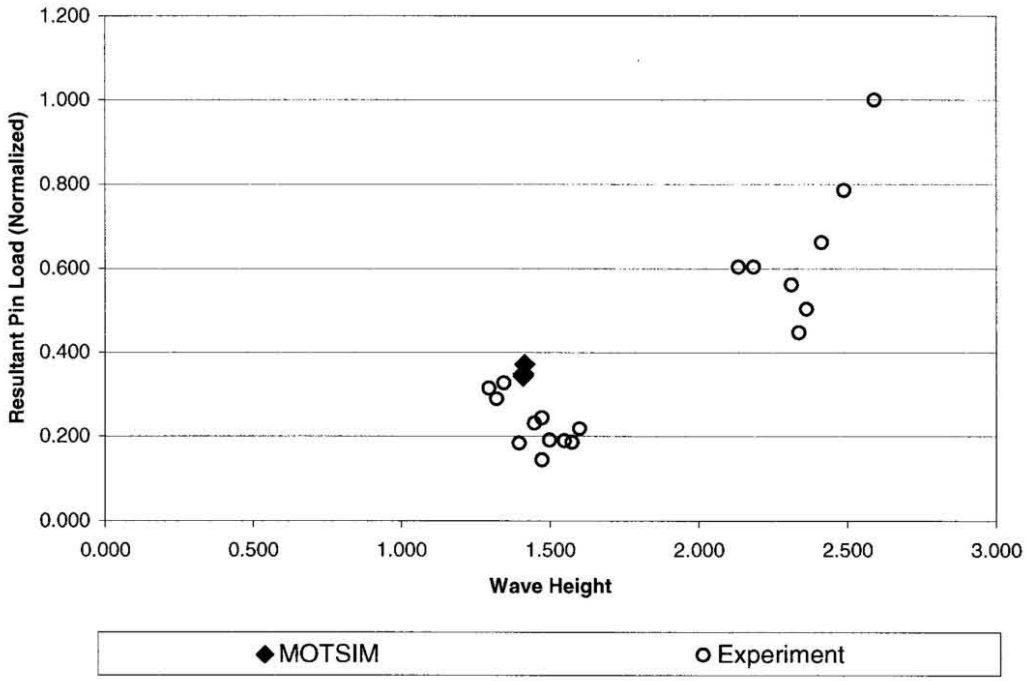

Figure 59: Comparison of ATB Resultant Pin Loads for Head Seas

5.5 Conclusion

The results presented in this chapter indicate that the MOTSIM time-domain seakeeping code has potential for application to Articulated Tug Barge units. The implementation of holonomic constraints with projection proved adequate to model the

pinned joint for short term simulations, but was unstable in longer term simulations as needed for irregular waves. Further investigation of the constraint configuration is required. The simulation may be more stable with a full implementation of the holonomic constraints rather than the hybrid scheme used here in which MOTSIM's internal restraining code was used for roll and yaw. It was also found that care must be taken to ensure that the constraint matrix is not ill conditioned. In the present case, it was possible to scale the problem to achieve a satisfactory result, but this procedure may not be generally applicable and other means of conditioning this matrix may be required.

Based on these results, it seems likely that MOTSIM could be used in other applications involving multiple floating bodies with mechanical constraints. Such applications may include tanker lightering operations, escort tug operations in a seaway, or heavy lift vessels. Successful application to more general multi-vessel problems will require that the hydrodynamic interaction forces be included in the simulations. This will require significant additional research and validation.

Chapter 6

Conclusion

The motions of two types of multiple waterplane vessels were simulated using the time-domain seakeeping simulation software package, MOTSIM. It was shown that, with its recent modifications, MOTSIM's output compared well with experimental data for a triangular semi-submersible. During the process of preparing these simulation results, several problems were identified and the procedure for simulating such complex vessels was modified. Specifically, it was shown that it is not acceptable to use facing panels at the interface of multiple components due to errors in the solution radiation potential. Instead, matched, or nearly matched, panel interfaces are required throughout the surface mesh. The importance of mesh quality becomes even more important when the motions of the vessel are unknown. Clearly, further validation studies must be carried out to verify MOTSIM's performance for these vessels, but these initial data are very encouraging.

A new version of MOTSIM has been developed to simulate two floating bodies. This version also allows for the inclusion of mechanical constraints between the vessels. To

validate this version of the code, the motions of an Articulated Tug Barge (ATB) were simulated in regular and irregular head seas. Comparison of the connection forces and relative pitch motions for the tug and barge show promise for the application of the method. Incomplete information from the model tests prevented adequate verification of the model and time constraints limited the number of simulations which were performed. Further comparisons are necessary to validate the code for this type of application. Also, numerical instability in the constraint formulation limited the duration of the simulations. Additional research is required to determine a more appropriate method of stabilizing the constraint model.

In summary, it was shown that MOTSIM is adaptable to a variety of non-standard seakeeping applications with complex vessel geometry and that the simulated results for the cases tested compare well with data from model experiments. While further validation work is required, this package has significant potential as an engineering design tool for complex marine vessels.

References

Abramowitz, M. and Stegun, I.A., Handbook of Mathematical Functions with Formulas, Graphs and Mathematical Tables, Dover Publications, New York, 1964

Bass, D.W., "Simulation of Ship Motions in the Time Domain", Prepared under contract to National Research Council of Canada, July 1988

Beck, R.F., "Ship Responses to Regular Waves", Principles of Naval Architecture, Vol.3, pp.41-83, SNAME, 1989

Borodai, I.K. and Netsvetayev, Y.A., Ship Motions in Ocean Waves, (in Russian), Sudostorenie, 1969

Edwards, C.H, Jr., and Penney, D.E., Calculus and Analytic Geometry, 3rd Edition, Prentice Hall, 1990

Faltinsen, O.M., Sea Loads on Ship and Offshore Structures, Cambridge University Press, Cambridge, UK, 1990

Frank, W., "Oscillation of Cylinders in or Below the Free Surface of Deep Fluids", Report Number 2375, David Taylor Research Center, Bethesda, Maryland, 1967

Himeno, Y., "Prediction of Ship Roll Damping – State of the Art", No. 239, September 1981, The Department of Naval Architecture and Marine Engineering, University of Michigan

Harris, C.J., et.al., Oceanic Consulting Corporation, Report FGL004-01, 1999

JRME, "WAMIT-MOSES Hydrodynamic Analysis Comparison Study", J.Ray McDermott Engineering, LLC, July 2000

Lewis, F.M. (1929). The inertia of water surrounding a vibrating ship, *Trans. SNAME*, 27, 1-20

Marine Log, "Shuttle Tankers in the Gulf It's as easy as ATB", http://www.marinelog.com/DOCS/PRINT/shutt2.html, 2000

Morison, J.R., O'Brien, M.P., Johnson, J.W. & Schaaf, S.A. "The Force Exerted by surface waves on piles", Pet. Trans., 1950

Newman, J.N., "Algorithms for the Free Surface Green Function", Journal of Engineering Mathematics, 1985

Ogilvie, T.F., "Recent Progress Toward the Understanding and Prediction of Ship Motions", Proceedings, 5th Symposium on Naval Hydrodynamics, ONR, Washington, D.C., 1964

Pawlowski, J.S., Bass, D.W. and Grochowalski, S., "A Time Domain Simulation of Ship Motions in Waves", Proceedings of the Seventeenth Symposium on Naval Hydrodynamics, 1988, pp.579-610

Pawlowski, J.S. and Bass, D.W., "A Theoretical and Numerical Model of Ship Motions in Heavy Seas", SNAME Transactions, Vol. 99, 1991, pp. 319-352

Saletan, E.J. and Cromer, A.H., Theoretical Mechanics, John Wiley & Sons, 1971

Salvesen, N., Tuck, E.O. and Faltinsen, O. (1970). Ship motions and sea loads, *Transactions Society of Naval Architects and Marine Engineers.* Vol 78, 250-287.

Sen, D., Doctoral Thesis, Memorial University of Newfoundland, 1988

Söding, H., "Eine Modifikation der Streifen-methode", Schiffstechnik, Bd. 16, Heft. 80, 1969

Stern, F. et.al., "http://www.iihr.uiowa.edu", 2001

St. Denis, M. and Pierson, W.J., "On the Motions of Ships in Confused Seas", SNAME Transactions, Vol. 61, 1953

Tanaka, N., "A Study of the Bilge Keels (Part 4 – On the Eddy-Making Resistance to the Rolling of a Ship Hull)", Journal of the Society of Naval Architects of Japan, Vol. 109, 1960

Tasai, F. and Takaki, M., "Theory and Calculation of Ship Responses in Regular Waves", (in Japanese), Symposium, Seaworthiness of Ships, Society of Naval Architects of Japan, 1969

Ursell, F. (1949). On the heaving motion of a circular cylinder in the surface of a fluid, *Quart. J. Mech. Appl. Math.*, 2, 218-231

Wehausen, J.V. and Latoine, E.V., "Surface Waves", Handbuch der Physik, Vol.9, pp.446-778, Berlin, 1960